JOURNAL OF GEOPHYSICAL RESEARCH, VOL. 102, NO. B9, PAGES 20,551–20,570, SEPTEMBER 10, 1997

Stability of a frictional, cohesive layer on a viscous substratum: Validity of asymptotic solution and influence of material properties

N. Triantafyllidis

Department of Aerospace Engineering, University of Michigan, Ann Arbor

Y. M. Leroy

Laboratoire de Mécanique des Solides, CNRS URA 317, Ecole Polytechnique, Palaiseau, France

Abstract. This study deals with the stability of a stratified structure composed of a cohesive and frictional overburden, a viscous substratum, and a rigid basement. That structure should be seen as a prototype for various salt tectonics and lithospheric plates stability analyses. The destabilizing factors are the density contrast, the tectonic compressive stress, and the possible erosion and deposition at the top surface. The overburden stiffness, a nonlinear function of in situ stress, has a stabilizing role. Two solutions are extracted from the variational formulation of the stability problem previously proposed [*Leroy and Triantafyllidis*, 1996]: the first is analytical and is obtained by disregarding gravity, and the second is numerical and is based on the finite element method. The latter is used to assess the validity of the previously presented asymptotic solution. It is shown that the asymptotic solution is accurate even for values of the small parameter, defined as the perturbation wavenumber times the overburden thickness, as large as 0.4. Furthermore, the possibility for the cohesive material in the overburden to accommodate part of the deformation by slip along a population of small pervasive faults is accounted for by the introduction of a deformation theory of plasticity. Stability predictions based on this theory indicate that structural modes, such as folding, and localized faulting modes are triggered for similar stress magnitudes. The parametric study presented includes the previously undetected influences of the stress gradient with depth and of the work hardening properties of the competent overburden. The role of erosion and deposition in destabilizing shallow overburdens, regardless of the magnitude of the tectonic stress, is also established. The stability predictions are then applied to a folded section through the Campos basin, offshore Brazil, revealing that the deformation theory of plasticity is necessary to explain the buckling that occurred during the Albian.

Introduction

The model considered here and by *Leroy and Triantafyllidis* [1996] consists of a cohesive, frictional overburden overlaying a viscous substratum of finite thickness and lower density and a rigid basement. The choice of an elastoplasticity model for the mechanical response of the overburden material renders possible the concurrent analysis of two sets of instabilities. The first set consists of diffuse modes, such as folding in compression and necking in extension, detected from the solution of an eigenvalue analysis for the whole stratified system. Shear band mode of instability constitutes the second set and marks the onset of localized faulting which is detected by the local condition of loss of ellipticity of the governing equations.

The motivation for solving the buckling problem of elastoplastic layers has several origins, discussed at length by *Leroy and Triantafyllidis* [1996], and only two points of interest are briefly mentioned here. First, the role of the density contrast, the tectonic forces and the overburden stiffness in driving salt diapirism in sedimentary basins have been studied traditionally in the laboratory [*Nettleton and Elkins,* 1947] and more recently by numerical means [*Poliakov et al.,* 1993; *Daudré and Cloetingh,* 1994]. Our stability analysis complements these earlier works by quantifying the influence on stability of the nonlinear work hardening properties of the frictional and cohesive overburden material which is either difficult to scale for granular materials in the nonlin-

Paper number 97JB01442.
0148-0227/97/97JB-01442$09.00

ear range of deformation or disregarded for numerical reasons. This line of work should be completed with the introduction of a rheological model for the basement and could then contribute to the elucidation of the role played by tectonics forces and density contrast in the formation of salt structure during thin- or thick-skinned compression in sedimentary basins [*Vendeville and Jackson,* 1992; *Stewart and Coward,* 1996]. Second, studies of the oceanic lithosphere recognize that the upper layers yield and thus do not contribute to the bending strength in an elastic manner [*McAdoo and Sandwell,* 1985]. Such an idea was explored by *Wallace and Melosh* [1994], who studied numerically the buckling of a pervasively faulted lithosphere with the model of an elastic plate in which faults were accommodating slip with no friction. An alternative approach is to smear those faults over the top part of the lithosphere and to make use of an elastoplasticity model such as the one considered here to introduce dissipation. It should be stressed that initiation of buckling for elastoplastic solids occurs in general under increasing load and is thus initially stable in a force-control set up [*Shanley,* 1947; *Hill,* 1958]. The buckling of geological structures modeled with the theory of plasticity is unlikely to lead to the catastrophic failure discussed by Wallace and Melosh and thus deserves further attention.

Leroy and Triantafyllidis [1996] (hereinafter referred to as paper 1) presented a variational formulation of the stability problem to detect diffuse modes of instability. It is applicable to a general class of strain rate independent plasticity models for the cohesive, frictional overburden material. The timescale relevant to the structure's stability is associated with the substratum viscosity. However, the details of the substratum rheology are not important since the passive compression necessary to detect nonlinear viscosity effects [*Sherwin and Chapple,* 1968; *Fletcher,* 1974] is disregarded and time independent equilibria assumed. An asymptotic solution to that variational formulation was presented for an overburden thickness which is small compared to the perturbation wavelength. This solution differs from previously published asymptotic solutions [*e.g., Smolu-*

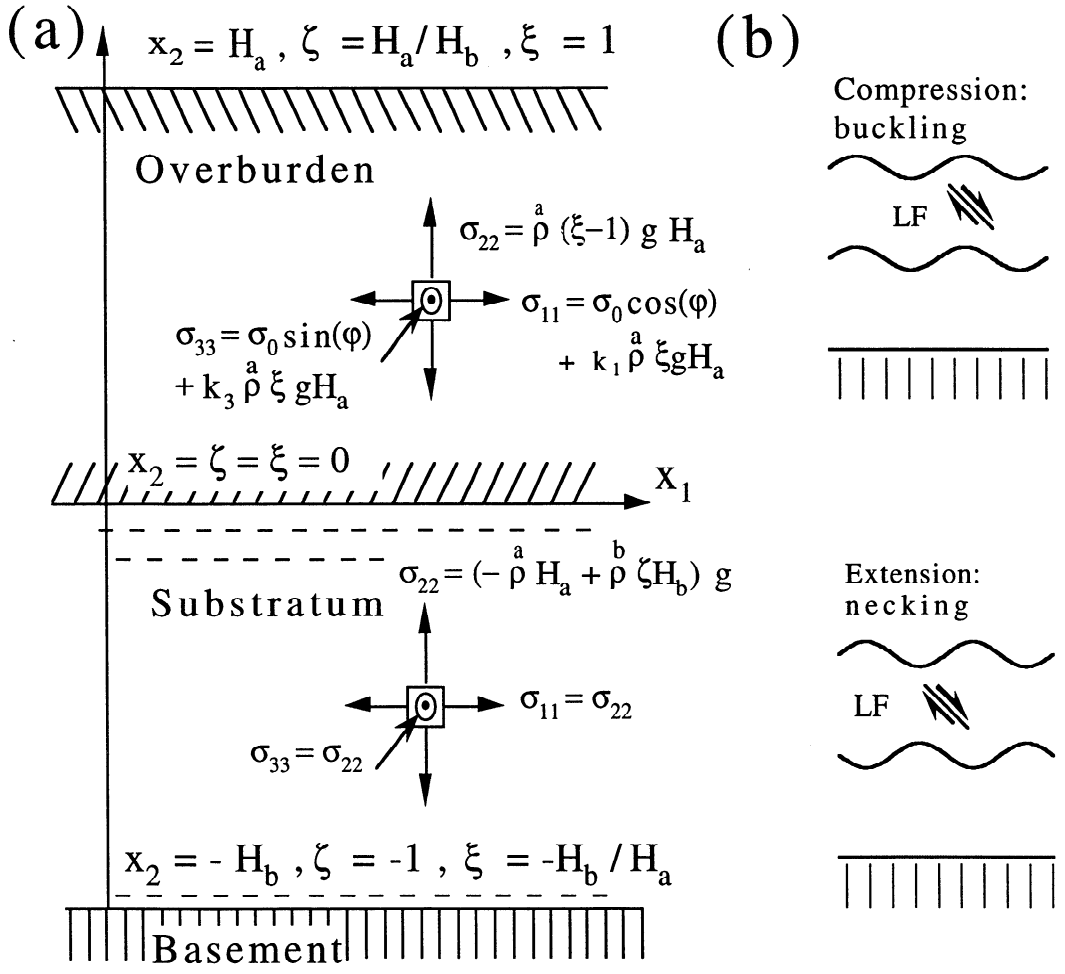

Figure 1. Geometry of the problem, in situ stress distribution, and illustration of some of the instability modes studied. (a) The overburden, composed of a frictional, cohesive material, lies on a layer of viscous fluid. The two strata are above a rigid basement. The overburden sustains its own weight and a tectonic stress distribution characterized by the stress parameter σ_0, the gradient coefficients k_1 and k_3, and the orientation angle φ. The state of stress in the substratum is hydrostatic. (b) Two structural modes of instability are illustrated together with the mode of localized faulting (LF).

chowski, 1909] by the nonlinear response of the overburden, the presence of a stress gradient with depth, and the erosion and redistribution condition [*Biot and Odé,* 1965] at the top surface. Results for the onset of folding mode of instability have been presented for the flow theory version of the plasticity model of *Rudnicki and Rice* [1975]. It was found that there is a range of lateral compressive stress, which includes the domain of elastic response, for which the system is stable to perturbations of any wavelength despite the density contrast. The conditions for neutral stability are not affected by the precise nature of the boundary conditions between substratum and basement. However, in the unstable range of stress, these boundary conditions are found to be important if the perturbation wavenumber times the substratum thickness is smaller than 4. In that instance, the thinner the substratum, the slowest the initial rate of growth of the instability. A condition of perfect bond with the basement reduces that rate compared to a condition of slip with no friction.

This paper has two objectives. First, it is necessary to define the range of validity of the asymptotic solution discussed above. For that purpose, a finite element solution of the variational formulation is proposed which approximates with the appropriate accuracy the exact solution which could not be obtained analytically because the material coefficients are varying spatially through the overburden. It is only in the absence of gravity that such an analytical solution is derived. Second, assessment is made of the influence on stability of the various parameters of the plasticity model adopted for the overburden. We have previously shown that the use of the flow theory version of *Rudnicki and Rice*'s [1975] model is appropriate to detect the onset of folding but not of localized faulting, even if a weak work hardening is adopted. The fact that these two modes of instability are not concomitant questions the relevance of the flow theory version of Rudnicki and Rice's plasticity model for the problem treated. Indeed, it appears that a deformation theory of plasticity, which mimics the effects of pervasive small faults in accommodating permanent bulk deformation, would be more appropriate to trigger diffuse modes and localized faulting for realistic stress conditions [*Triantafyllidis and Leroy,* 1994]. This distinction between flow and deformation theory of plasticity deserves some clarification in the present context of a geological stability analysis at the tectonic scale and such a discussion is given herein and by *Leroy and Triantafyllidis* [1997].

The contents of this paper are as follows: In the second section, the model problem and its stability variational formulation are summarized including a discussion on the incremental response of the overburden material. The solutions to the stability problem are also summarized, and the details of the numerical solution based on the finite element method and of the analytical solution obtained in the absence of gravity are postponed to the appendix. The third section is devoted to the application of these solutions to *Rudnicki and Rice*'s [1975] constitutive model. The range of validity of the asymptotic solution is established: its accuracy is excellent as long as the small parameter of the analysis, defined as the overburden wavenumber times the overburden thickness, is less than 0.4. That section also contains a comparison between predictions based on flow and deformation theories. The deformation theory is found necessary to explain the initiation of localized faulting and folding under stress magnitudes of similar order. These solutions are then applied in the fourth section to a prototype, with a geometry identical to the one described above, proposed for a section revealed by a seismic dip line through the Campos basin off the southeastern Brazilian coast [*Cobbold and Szatmari,* 1991]. An interpretation of the two stages of buckling in the absence of localized faulting, in the Albian and in the Tertiary, is presented. It requires the application of the deformation theory of plasticity to explain folding for the stress conditions that must have prevailed in the field.

Model Problem

This section is devoted to the presentation of the model and to a summary of the hypotheses introduced during the derivation of the variational formulation of the stability problem developed in paper 1. The solutions to that stability problem, which are also discussed, provide the conditions for the onset of diffuse instabilities such as folding in compression and necking in extension (Figure 1b).

Model Formulation

The stratified system considered is composed of three regions of infinite lateral extent referred to as the overburden, the substratum, and the rigid basement (Figure 1a). Thicknesses and densities of the overburden and substratum are denoted by H_a, ρ_a and H_b, ρ_b, respectively. In what follows, any material or geometric parameter or field variable related to one of the two layers has superscript or subscript a or b, indicating above and below, respectively. The coordinate system is such that the first and third axes are within the planar interface between substratum and overburden; the x_2 coordinate axis is oriented vertically. The coordinates ξ and ζ, introduced for convenience, are defined by normalizing x_2 by the overburden and substratum thickness, respectively.

The in situ stress state in the stratified system is Andersonian, as indicated in Figure 1a. The sign convention is that compressive stresses are negative. The stress component in directions 1 and 3 varies linearly with depth having a gradient k_1 and k_3 times the lithostatic pressure, respectively. The stress at the interface between the two layers has magnitude $\sigma_0 \cos(\varphi)$ and $\sigma_0 \sin(\varphi)$ along the 1 and 3 axis, respectively. A variation of φ from zero to $\pi/2$ leads to a change from a state of uniaxial compression along the 1 axis to a similar loading along the 3 axis. The stress state in the substratum results solely from the overburden weight and the hydrostatic pressure. Note that pore pressure effects are disregarded in this analysis. This hypothesis

is common to paper 1 and is justified for systems fully drained on the geological timescale of interest.

Stability analyses require the knowledge of the material's incremental response. Typically, the overburden material results from the deposition of sediments which then sustain a mechanical and chemical compaction under varying tectonic forces, temperature, and fluid pressure. This history, often unknown, determines the incremental response measured in the laboratory from a core extracted from the field. To circumvent this complexity, it is proposed to determine the incremental response at any point through the thickness of the overburden from the results of a single laboratory test from which a uniaxial stress-strain curve such as the one depicted in Figure 2 is obtained. As a consequence, temperature effects on the material response, which could be accounted for in the constitutive model, are disregarded in this analysis. The curve in Figure 2 presents an equivalent stress measure as a function of the accumulated equivalent strain; the exact definitions of these stress and strain measures will be provided later and are not important for the present discussion. It suffices to know that at every point in the overburden the equivalent stress is uniquely determined from the stress parameterization discussed above. The curve in Figure 2 shows a linear relation if the equivalent stress is less than the yield stress τ_y which plays a role similar to a cohesion. For stress larger than this critical value,

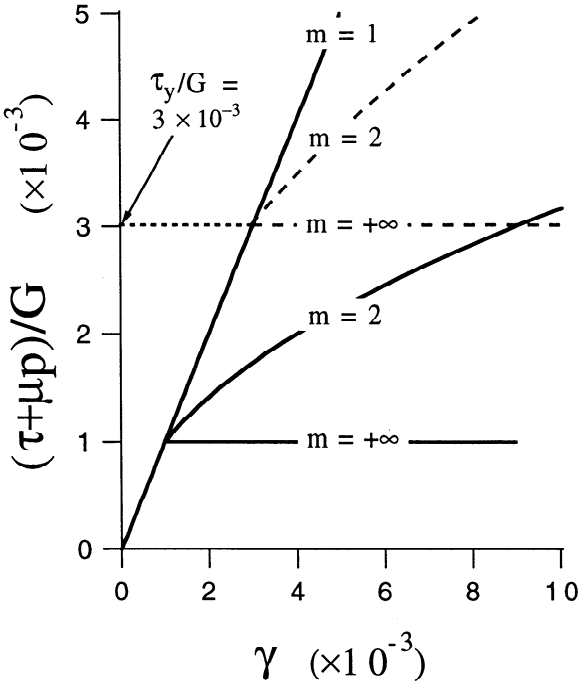

Figure 2. The uniaxial stress-strain curve of the overburden material is linear for an equivalent stress less than the yield stress τ_y which has for value either $G \times 10^{-3}$ (solid curves) or $3G \times 10^{-3}$ (dashed curves). This relation becomes a power law with exponent m if the initial yield stress is exceeded. The two values for m of 1 and $+\infty$ corresponds to an elastic and an elastic, perfectly plastic response, respectively.

the relation is nonlinear due to a positive work hardening but always one-to-one, such that a unique equivalent strain is associated to any value of the equivalent stress.

With these hypotheses, and the further assumption that the current stress state has been reached while keeping constant the directions and ratios of principal stresses (proportional loading), the incremental response of the material is then fully determined. It is represented by a fourth-order tensor $\overset{a}{L}_{ijkl}$ which relates the time derivative (denoted by an overdot) of the second Piola-Kirchhoff stress tensor Π_{ji} to the same derivative of the displacement gradient $u_{i,j}$

$$\dot{\Pi}_{ji} = \overset{a}{L}_{ijkl}\, \dot{u}_{l,k} \qquad 0 \le x_2 \le H_a\,. \tag{1}$$

The reader is referred to standard continuum literature for the definition of the Piola-Kirchhoff stress tensor and for its relation to the Cauchy stress tensor introduced for the in situ stress parameterization [*e.g., Ogden,* 1984]. Expressions for the moduli $\overset{a}{L}_{ijkl}$ are provided by *Rudnicki and Rice* [1975] for both flow and deformation theories. A derivation of these moduli plus a physical motivation for the use of deformation theories are given by *Leroy and Triantafyllidis* [1997]. It should be stressed that the curve in Figure 2 is obtained for both the flow and deformation theory version of the same plasticity model. These two theories lead to the same moduli in the direction of proportional loading which is followed during the test conducted to obtain that curve.

Stability Analysis

The derivation of the variational formulation of the stability problem presented in paper 1 is now summarized to recapitulate the various hypotheses considered. The starting point of the derivation is the rate form of the equilibrium equations in the overburden and substratum, the traction and velocity continuity equations at the interface of the overburden and substratum, the redistribution condition at the free surface, and two types of boundary conditions at the basement. The two possibilities considered are, first, perfect bond and, second, slip with no friction. The introduction of a simple erosion and deposition condition at the free surface follows the model of *Biot and Odé* [1965] which relates the normal component of the traction vector to the weight of the volume of material displaced

$$\dot{\Pi}_{2j} = s\, \overset{a}{\rho}\, g \dot{u}_2 \delta_{j2} \quad \text{at} \quad x_2 = H_a\,, \tag{2}$$

in which δ_{ji} and g are the Kronecker delta (equal to one if i and j are identical and to zero otherwise) and the gravity acceleration. This relation indicates that a positive traction results from a top surface which is upheaved and thus should be eroded away, while a compression is applied to the region which subsided due to the addition of new sediments of the same density as the overburden material. The scalar s in (2) is set to one if redistribution is accounted for and leads to a stress-free boundary condition if a zero value is chosen.

All perturbations considered in this linear stability analysis are superposed to the fully three-dimensional stress state but satisfy the simplifying conditions of plane strain. Any perturbed state fulfills throughout the overburden the plastic flow conditions set by the in situ stress: if permanent deformation is necessary to accommodate the in situ stress prescribed at a given material point, then the perturbation can only induce further plastic straining. Possible elastic unloading in regions of the overburden upon perturbation are thus disregarded in this linear analysis. This choice is equivalent, for the overburden, to the selection of a "comparison solid" usually employed for detecting the first bifurcation in solids [*Hill,* 1958] and structures [*Shanley,* 1947]. The validity of this hypothesis is verified from the results of a nonlinear stability analysis based on the finite element method [*Massin,* 1995; *Massin et al.,* 1996].

The variational formulation of the stability problem constitutes a generalized eigenvalue problem and takes the final form

$$\int_0^1 \Big[\Big(\frac{\overset{a}{L}_{1221}}{\omega H_a}\frac{dU_1}{d\xi} + \overset{a}{L}_{1212}U_2\Big)\frac{1}{\omega H_a}\frac{d\delta U_1}{d\xi} - \Big(\frac{\overset{a}{L}_{1122}}{\omega H_a}\frac{dU_2}{d\xi} - \overset{a}{L}_{1111}U_1\Big)\delta U_1 + \Big(\frac{\overset{a}{L}_{2222}}{\omega H_a}\frac{dU_2}{d\xi} - \overset{a}{L}_{2211}U_1\Big)\frac{1}{\omega H_a}\frac{d\delta U_2}{d\xi} + \Big(\frac{\overset{a}{L}_{2121}}{\omega H_a}\frac{dU_1}{d\xi} + \overset{a}{L}_{2112}U_2\Big)\delta U_2\Big]d\xi - \frac{1}{(\omega H_a)^2}\Big[s\,\overset{a}{\rho}\,gH_aU_2\delta U_2\Big]_{\xi=1} + \frac{1}{\omega H_a}\Big[\overset{a}{\rho}\,gH_a(U_1\delta U_2 + U_2\delta U_1) + \frac{\overset{b}{\rho}\,gH_b}{\omega H_b}U_2\delta U_2\Big]_{\xi=0} + \frac{\Lambda}{\omega H_a}\Big[(f_{11}U_1 + f_{12}U_2)\delta U_1 + (f_{21}U_1 + f_{22}U_2)\delta U_2\Big]_{\xi=0} = 0\,. \qquad (3)$$

The eigenvector of components U_i together with the wavenumber ω define the perturbation of interest. The eigenvalue of the problem is the stability exponent Λ which has, with the present notation, dimension of stress and whose real part is the rate of growth or decay of the perturbation. If there is an eigenvector U_i for which Λ has a positive real part, then the equilibrium is said to be unstable. Stability requires all admissible eigenvectors to have a Λ with negative real part. Neutral stability is defined for a zero value of that quantity. The four functions f_{ij} of the substratum's dimensionless thickness ωH_b introduced in (3) represent the influence of the viscous substratum assumed to be incompressible with an elastic moduli which can be disregarded compared to the in situ stress. These functions depend on the type of boundary condition at the substratum-basement interface. For a perfect bond, they are given by

$$f_{11} \equiv \frac{\cosh(\omega H_b)\sinh(\omega H_b) - \omega H_b}{\sinh^2(\omega H_b) - (\omega H_b)^2}\,,$$

$$f_{12} \equiv \frac{-(\omega H_b)^2}{\sinh^2(\omega H_b) - (\omega H_b)^2} \equiv f_{21}\,,$$

$$f_{22} \equiv \frac{\cosh(\omega H_b)\sinh(\omega H_b) + \omega H_b}{\sinh^2(\omega H_b) - (\omega H_b)^2}\,, \qquad (4)$$

and by

$$f_{11} \equiv \frac{\sinh^2(\omega H_b)}{\cosh(\omega H_b)\sinh(\omega H_b) - \omega H_b}\,,$$

$$f_{12} \equiv \frac{-\omega H_b}{\cosh(\omega H_b)\sinh(\omega H_b) - \omega H_b} \equiv f_{21}\,,$$

$$f_{22} \equiv \frac{\cosh^2(\omega H_b)}{\cosh(\omega H_b)\sinh(\omega H_b) - \omega H_b}\,, \qquad (5)$$

for the case of slip with no friction. Note from (3) that the solution to the stability variational formulation at neutral stability ($\Lambda = 0$) is independent of the function f_{ij} (and thus of the depth of the substratum and the boundary conditions with the basement). Note also that for an infinitely deep substratum, these functions are nothing but the Kronecker functions δ_{ij} found by *Triantafyllidis and Leroy* [1994].

The predictions resulting from that variational formulation are valid in the elliptic regime of the incremental governing equations. The loss of ellipticity corresponds to the initiation of a discontinuity in the velocity gradient which is interpreted as the onset of localized faulting [*Rudnicki and Rice,* 1975]. That condition is local in the sense that only the stress state and the incremental moduli are required for its application at a given point of the overburden. Equation (29) of *Triantafyllidis and Leroy* [1994] is used for checking that condition in the following.

Solutions to the Stability Problem

See the appendix for the details of the derivations of two solutions of the stability problem presented in (3) to (5). The first is analytical and obtained in the absence of gravity effects. The second is numerical and based on the finite element method. Both contribute to the validation of the asymptotic solution which is now briefly reviewed to help us in analyzing the results presented in the next section.

To compensate for the absence of an analytical solution to our stability problem, paper 1 proposed construction of an asymptotic solution for a dimensionless number ωH_a small compared to one. The construction of the long-wavelength approximation starts from the observation that the dimensionless number $\Delta\rho g/\omega G$, interpreted as a function of Λ, admits a development of the type

$$\frac{\Delta\rho g}{\omega G} = \gamma_0 + \epsilon\gamma_1 + \epsilon^2\gamma_2 + \epsilon^3\gamma_3 + \mathcal{O}(\epsilon^4)\,, \qquad (6)$$

in which ϵ, the small parameter, is the dimensionless number ωH_a. In (6), $\Delta\rho$ and G denote the material density difference $(\overset{a}{\rho} - \overset{b}{\rho})$ and the modulus of elasticity

in shear of the overburden material, respectively. The unknown scalars γ_α are functions of Λ. The details of the derivation are found in the electronic supplement to *Leroy and Triantafyllidis* [1996]. Note that this development is constructed for constant value of the ratio Λ/ϵ denoted by Λ_1 in the following. Asymptotic development for constant value of Λ, and not Λ_1, is impossible due to the presence of singularities close to the neutral stability conditions (see paper 1 for further discussion). The expression proposed in (6) takes the more familiar form

$$\frac{\Lambda}{G} = \frac{\Delta\rho g}{\omega G} - \epsilon\frac{\sigma_0}{G} - \epsilon^3\frac{1}{6(1-\nu)}, \qquad (7)$$

in the restricted context of an elastic plate on an infinitely deep viscous foundation. The rate of growth of the instability is influenced by the density contrast, the tectonic stress, and the plate bending stiffness; these contributions being to the zero-, first-, and third-order in the small parameter ϵ. The asymptotic development in (6) extends this classical solution (7), discussed by *Ramberg and Stephansson* [1964] and *Smoluchovski* [1909] for Λ equal to zero, to the case of an elastoplastic overburden sustaining a tectonic stress with an arbitrary linear distribution with depth and resting on a substratum of finite thickness.

Results

This section is in four subsections, with the first presenting the material and geometric parameters employed for all calculations. The second deals with the validation of the asymptotic solution for several substratum thicknesses and for the two types of boundary conditions at the basement. The third is devoted to a comparison between stability predictions based on flow and deformation theory versions of *Rudnicki and Rice*'s [1975] model. A short discussion on the relevance of the deformation theory of plasticity in this linear stability analysis is included. The fourth pertains to the sensitivity of the stability predictions obtained with the deformation theory to the material hardening law, the in situ stress gradient, and the redistribution condition.

Preliminaries

The in situ stress state in the overburden is parameterized by the stress σ_0 at the interface with the substratum, the orientation angle φ, and the two scalars k_1 and k_3 which define the gradients with depth of the two horizontal stresses (see Figure 1a). The angle φ as well as the stress gradient parameters k_1 and k_3 are set to zero in the following, with the exception of the results in Figure 10 for which k_1 is set to 1 or 2.

The values chosen for all material parameters are similar to those considered in paper 1 and are typical of sedimentary rocks. The modulus of elasticity of the overburden material is 10^{10} Pa and its Poisson's ratio is 0.2. The initial yield stress τ_y is one thousandth of the elasticity modulus, unless otherwise stated. The yield criterion and plastic flow potential considered by *Rudnicki and Rice* [1975] depend on two constant scalars, the friction μ and the dilatancy coefficients. The dilatancy modeled here results from the opening of fracture during their sliding. Typically, during a triaxial test, the volume change is first negative and then positive prior to failure. A zero average value is thus chosen here in view of the simplicity of the micromechanism considered. Varying that dilatancy coefficient could be of interest for certain applications, such as in the next section for a sedimentary basin, only if a proper compaction law was proposed instead of the dilatancy induced by shear considered here. The friction coefficient is set to 0.6 which is typical of the values discussed by *Rudnicki* [1977].

The work hardening properties of the overburden material are parameterized by a power law (Figure 2) with an exponent m. In Figure 2, the equivalent stress $\tau+\mu p$ is the sum of the second invariant of the deviatoric part of the Kirchhoff stress τ and of the friction coefficient times the first invariant of that same tensor p. It is the generalization of the equivalent stress introduced by *Drucker and Prager* [1952] to large deformations. The equivalent strain is denoted by γ. Note that for m equal to 1 and infinity, the material response is purely elastic and elastic, perfectly plastic, respectively. Selecting a representative value for m from laboratory test results is difficult. The desired data sets should be obtained prior to maximum load to make sure that strain localization effects are not included [*Leroy and Ortiz*, 1989]. The selection of that exponent is also sensitive to the value taken for the first yield τ_y which is usually difficult to estimate. For these reasons, it is preferred here to chose an intermediate value for m of 5 for all calculations and to consider the influence of m by changing its value to 8 at a later stage. The latter value leads to large strain with little work hardening and is proposed to model poorly consolidated sediments or dry sand under low confining pressure. Such materials are considered in the next section.

The overburden and substratum material densities are supposed to be 2.5×10^3 and $2.2 \times 10^3 \mathrm{kg/m^3}$, respectively. Those values are close to the ones considered by *van Keken et al.* [1993]. Note that the substratum viscosity is not required explicitly here since equilibrium is assumed in the substratum: the viscosity scales with the stability exponent (see paper 1 for further discussion).

Before starting the discussion of our results, it is worthwhile to present the common features of the calculations and of the figures to be presented. Every graph is spanned by the normalized stress σ_0/τ_y and dimensionless number ωH_a. Each curve relates the critical stress σ_0/τ_y to the dimensionless overburden thickness or dimensionless perturbation wavenumber ωH_a necessary for a perturbation to grow at a given fixed rate. The curves in all graphs are thus isocontours of the stability exponent. Note again that for the asymptotic solution, it is not the stability exponent Λ/G which is kept constant but the scalar Λ_1/G, which is defined by $\Lambda = \Lambda_1\omega H_a$ and is referred to as the scaled stability ex-

ponent. A zero exponent, Λ or Λ_1, corresponds to the condition of neutral stability which partitions every plot into an unstable and a stable region, marked by a plus and a minus, respectively. Note that the finite element solution, shown by solid curves in all graphs, approximates the exact solution with an accuracy which is of the order of the graph resolution. For that reason, it is sometimes referred to as the exact solution in what follows. Calculations are always conducted for a constant value of one of the two dimensionless numbers $\Delta\rho g/G\omega$ and $\Delta\rho g H_a/G$. They differ by the characteristic length selected which is either the perturbation wavelength $2\pi/\omega$ or the substratum thickness H_a. In the case of a constant $\Delta\rho g/G\omega$, the observer keeps the perturbation wavelength constant and searches for the combinations of overburden dimensionless thickness ωH_a and lateral stress which trigger instability at a given rate. In the case of constant $\Delta\rho g H_a/G$, the observer keeps unchanged the overburden thickness H_a and varies the dimensionless perturbation wavelength ωH_a. Results obtained by the two methods differ because of the presence of a stress gradient in the overburden which depends on H_a but not on ω.

Validity of the Analytical and Asymptotic Solutions

The comparison of the analytical and asymptotic solutions to the numerical results is conducted for the flow theory version of *Rudnicki and Rice's* [1975] model. The case of an infinitely deep substratum and a 2π km long perturbation wavelength is first considered with $\Delta\rho g/G\omega$ having the value 7.06×10^{-4}. The isocontours of scaled stability exponent ($\Lambda_1 = \Lambda/\epsilon$) are plotted in Figure 3a. It is seen that the asymptotic solution (dotted curves) is indistinguishable from the exact solution (solid curves) even for values for ωH_a as large as 0.3. The range of validity of the asymptotic solution is surprisingly large since ωH_a is the parameter which is assumed to be small compared to one. The asymptotic solution thus captures perfectly the smallest magnitude of the critical stress σ_0 and the associated wavelength for neutral stability. These two quantities are the coordinates of the critical point on the neutral stability curve ($\Lambda_1 = 0$) where the tangent is vertical; it is the closest point to a vertical axis passing trough the origin of the σ_0 coordinate (not represented). The agreement between exact and analytical solutions (dashed curve) is satisfactory for large values of the dimensionless number ωH_a such as 0.8 but poor in the region of validity of the asymptotic solution. This is due to the improper account of the singular behavior for ωH_a close to zero of the analytical solution obtained in the absence of gravity. Note that the discontinuity in slope of the analytical solution at neutral stability marks the limit of an elastic stress response.

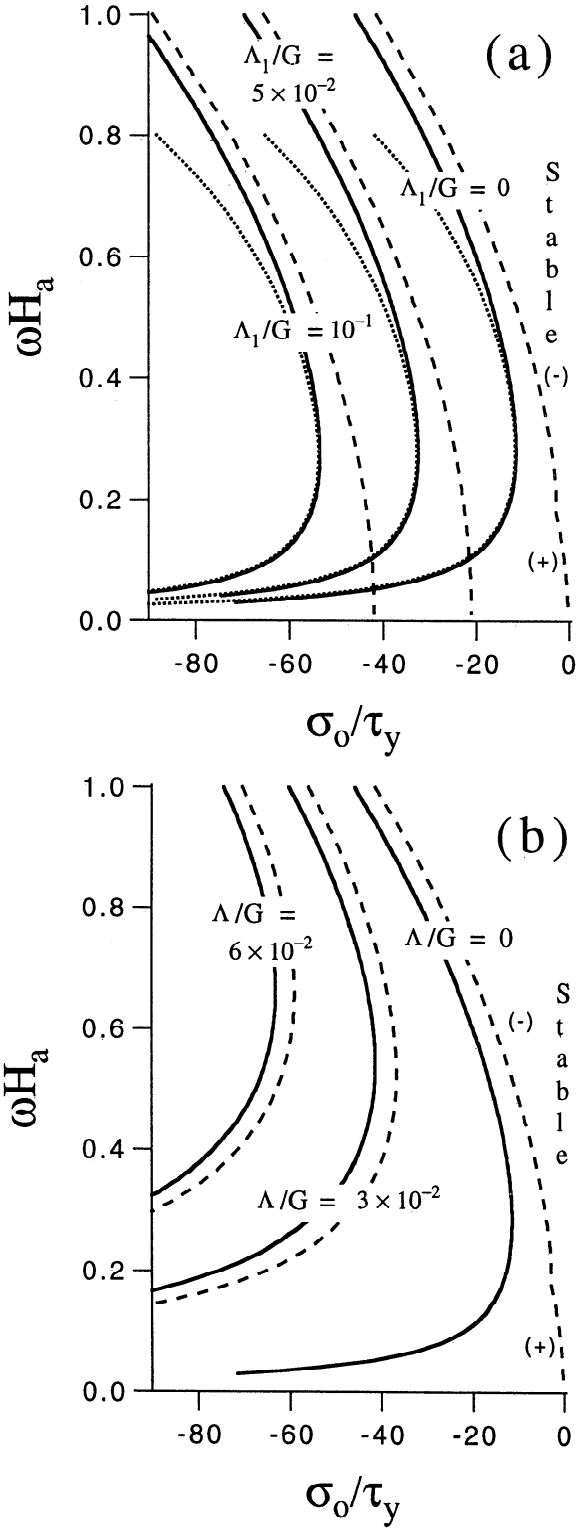

Figure 3. Comparison between stability predictions in a space spanned by the dimensionless thickness ωH_a and normalized stress σ_0/σ_y. Predictions obtained with the analytical solution in the absence of gravity (dashed curves), the finite element solution (solid curves), and the asymptotic solution for small values of ωH_a (dotted curves), the latter two accounting for gravity effects. The iocontours are drawn (a) for a constant value of the scaled stability exponent Λ_1 and (b) for a constant value of the stability exponent Λ. The two exponents are related by $\Lambda = \Lambda_1 \omega H_a$. Results are obtained for the flow theory version of *Rudnicki and Rice's* [1975] model for an infinitely deep substratum and for $\Delta\rho g/G\omega = 7.06 \times 10^{-4}$.

The parameterization adopted for the isocontours in Figure 3b is different: Λ is kept constant instead of Λ_1. Interestingly enough, this difference improves the validity of the analytical solution for small values of the dimensionless thickness ωH_a except close to neutral stability. These results are well understood by considering the isocontours that can be drawn from equation (7) for an elastic beam on an infinitely deep substratum. For large values of ωH_a, the bending stiffness of the elastic beam dominates and the isocontours are quadratic in ωH_a and similar to the curves drawn for the exact elastoplastic solution in Figure 3a. For vanishingly small values of ωH_a, the critical stress for the elastic beam behaves like one over ωH_a with a coefficient of proportionality equal to $(\Delta\rho g/(\omega G) - \Lambda/G)$. Note that this coefficient is zero if gravity is disregarded and the conditions of neutral stability fulfilled. The same trend is observed in Figure 3b (dashed line, $\Lambda = 0$) for the elastoplastic overburden. Note also from the same equation (7) that this singularity does not exist in the absence of gravity if the scaled stability growth rate Λ_1 is kept constant instead of Λ. This is exactly what happens for the dashed curves drawn for the elastoplastic overburden in the absence of gravity (Figure 3a).

The comparison between the three solutions of the stability problem is continued for the same 2π km long perturbation wavelength but now for a substratum of finite thickness, set to 1 and 5 km in Figures 4a and 4b, respectively. A perfect bond with the basement is imposed. The results concerning neutral stability are identical to the ones obtained for an infinitely deep substratum in Figure 3a. This independence of the neutral stability conditions on the substratum thickness and the choice of boundary conditions at the basement can be seen from the structure of the generalized eigenvalue problem (A7) as already discussed. Comparing Figures 4a, 4b, and 3a, we confirm one of the conclusions of paper 1 on the influence of the substratum thickness H_b: it becomes important once ωH_b is less than 5. Indeed, note that by decreasing the substratum thickness from 5 to 1 km, one reduces the instability exponent by a factor of 10. The confirmation of that earlier conclusion is now possible because of the excellent agreement between the asymptotic and exact solutions, even for large values of ωH_a (up to 0.3 to 0.4).

The influence of the substratum can also be judged from Figure 5 drawn for a constant dimensionless number $\Delta\rho g H_a/G$ of 7.06×10^{-4} obtained for an overburden thickness of 1 km. The substratum thickness has the same value in Figure 5a and is set to 5 km in Figure 5b, with the same perfect bond condition at the basement as in Figure 4. A comparison between the various isocontours in Figures 5a and 5b reveals that the stability exponent is 10 times larger for the 5 km thick than for the 1 km thick substratum. The dominant wavelength at a given compressive stress, defined by the value of ωH_a having the largest rate of growth, is varying, approximately, from 0.45 to 0.95 in Figure 5a and from 0.45 to 0.75 in Figure 5b. Close to neutral stability, the

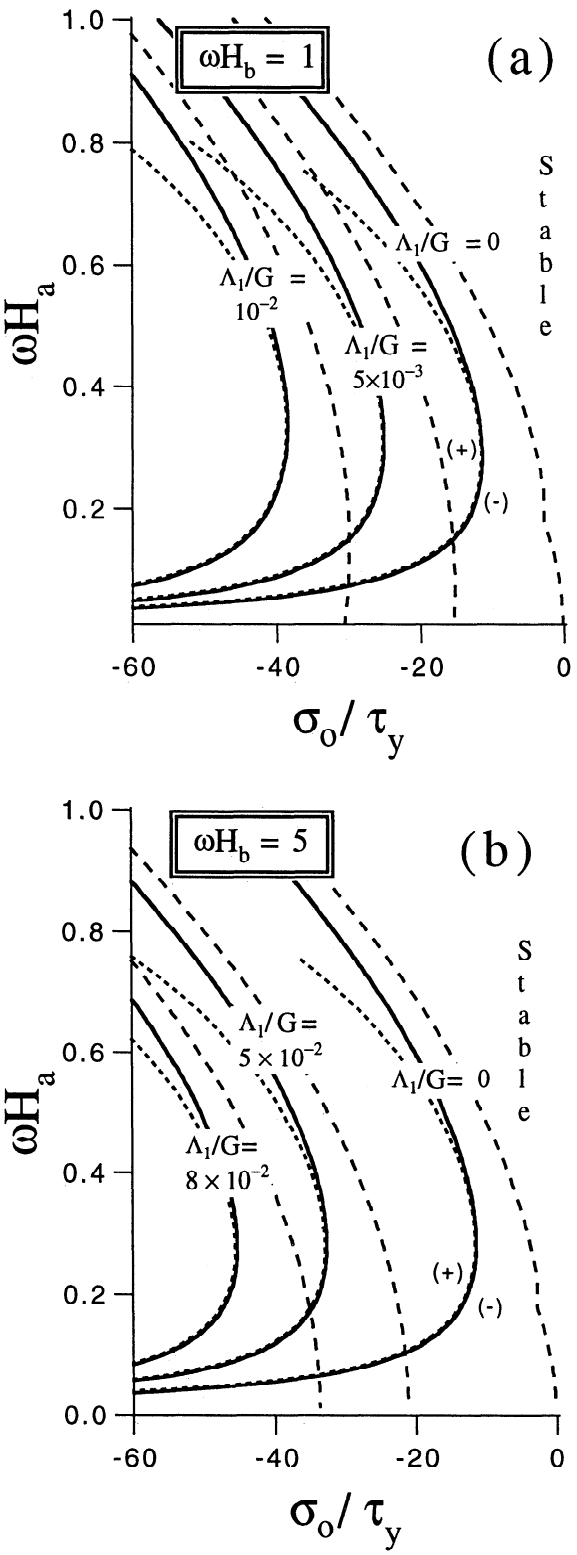

Figure 4. Influence of the substratum thickness on the stability of the stratified system according to the finite element (solid curves), asymptotic (dotted curves), and analytical (dashed curves) solutions for $\Delta\rho g/G\omega = 7.06 \times 10^{-4}$. The substratum thickness is set (a) to 1 km and (b) to 5 km. A thicker substratum implies a faster rate of growth of the instability for the same in situ stress. Results are obtained for flow theory and a perfect bond between substratum and basement.

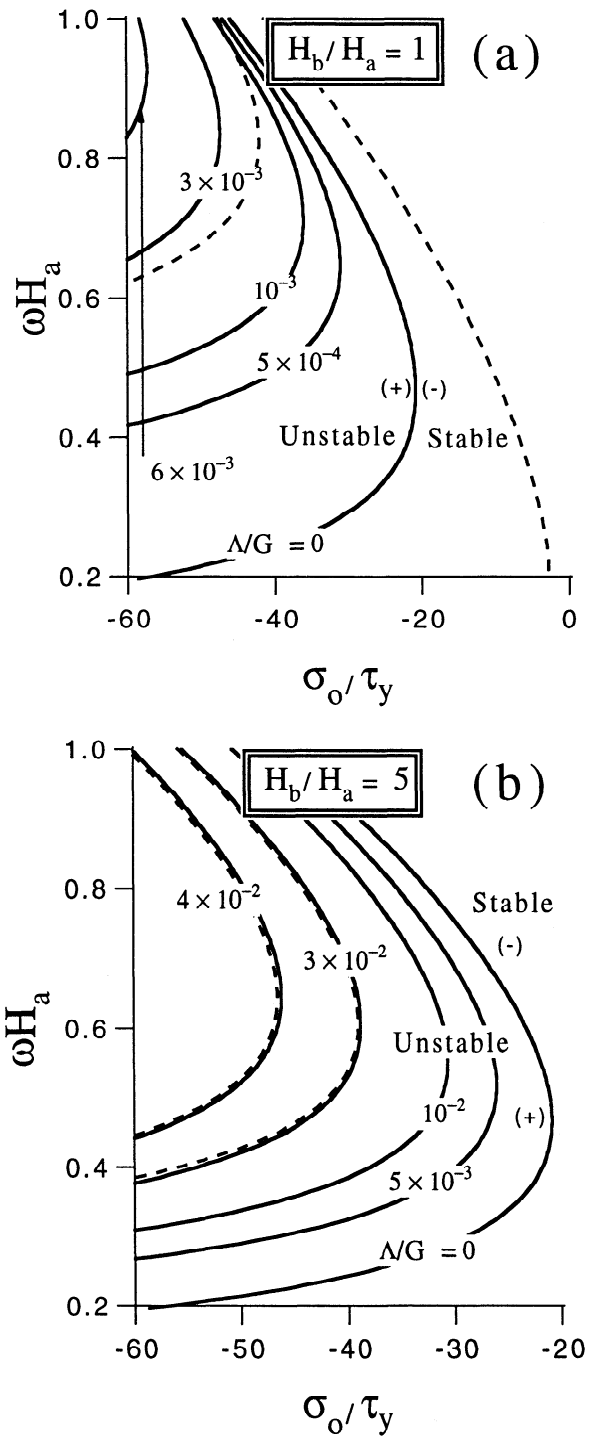

Figure 5. Influence of the substratum thickness for $\Delta\rho g H_a/G = 7.06 \times 10^{-4}$ obtained for an overburden thickness of 1 km. The isocontours of constant stability exponent Λ/G are drawn for a ratio of substratum to overburden thicknesses of (a) 1 km and (b) 5 km. Finite element, analytical, and asymptotic results are the solid, dashed, and dotted curves, respectively. Results are obtained for flow theory and a perfect bond between substratum and basement.

dominant wavelength is thus 14 km long and requires a minimum stress of $20\tau_y$. If the tectonic stress has a magnitude 3 times larger than this minimum, then the dominant wavelength becomes either 8.4 km or 6.6 km long for thick or shallow substratum, respectively. The substratum thickness thus influences the dominant perturbation wavelength by as much as 30% and its initial rate of growth by a factor 10. Note from Figure 5b that the analytical solution (dashed curves) is precise for a dimensionless rate of growth larger than or equal to 2×10^{-2}.

The comparison between analytical and numerical solutions is finalized with some comments on Figure 6, which illustrates the influence on stability of the condition of slip with no friction at the basement contact for a substratum thickness of 1 km. In Figure 6a, it is the perturbation wavelength which is kept to a constant length of 2π km, while the overburden has a constant thickness of 1 km in Figure 6b. These results should be compared with those presented in Figures 4a and 5a, respectively. That comparison reveals the stabilizing influence of the perfect bond at the basement. For example, the minimum stress to initiate an instability at a rate Λ_1/G of 10^{-2} is decreased approximately by a factor 2 from the perfect bond case of Figure 4a to the slip with no friction of Figure 6a. However, the dominant wavelength for a given stress σ_0 does not seem to be affected by the type of boundary condition (Figures 5a and 6b). The accuracy of the asymptotic solution is confirmed again in Figure 6a for the condition of slip with no friction. The analytical solution (dashed curves) provides the general trend of every contour, with the exception of the singularity for vanishing ωH_a for constant Λ_1.

It should be noted in concluding this subsection that all stability calculations reported so far fall within the elliptic regime of the incremental governing equations. Thus the onset of localized faulting was not detected even at compressive stresses 3 to 5 times larger (in magnitude) than the minimum one required to initiate folding. The next subsection questions this absence of localized faulting from our predictions and proposes to remedy this situation with the use of a deformation theory of plasticity.

Flow and Deformation Theories

Deformation theories of plasticity are used in linear stability and bifurcation analyses because they share a common feature with many micromechanically based plasticity theories. At the tectonic scale, the deformation theory version of *Rudnicki and Rice*'s [1975] model mimics the presence of randomly distributed small faults which accommodate the continuous macroscopic plastic deformation by combined slip. This enrichment of the deformation theory, as compared to the flow theory, leads to a reduction in the material stiffness in a direction perpendicular to the direction of proportional loading in stress space [*Stören and Rice*, 1975]. This reduction in stiffness facilitates any abrupt change in mode of deformation and thus the development of any instability such as faulting [*Rudnicki and Rice*, 1975]. Further discussion on deformation theories is given by *Leroy and Triantafyllidis* [1997]. The role of the defor-

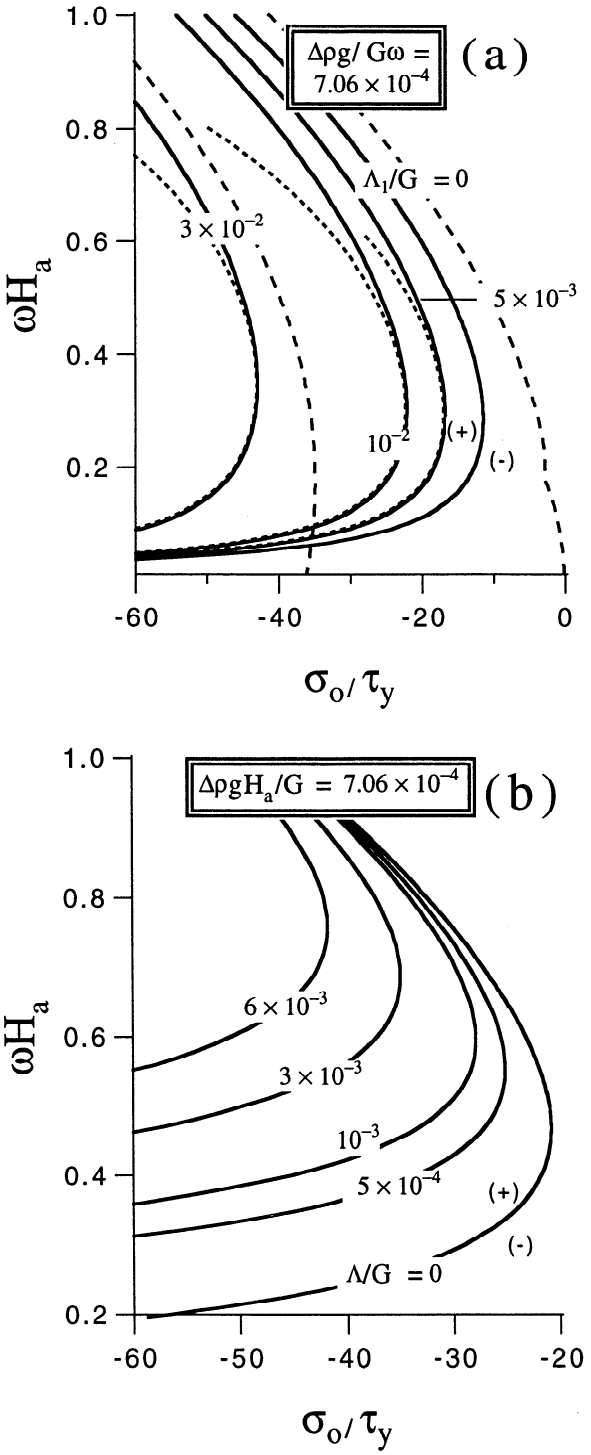

Figure 6. Influence of the boundary condition between substratum and basement. (a) The substratum thickness is 1 km and (b) the overburden thickness takes that same value. These results are obtained for a condition of frictionless slip and should be compared with those obtained for a perfect bond presented in Figures 4a and 5a. Finite element, analytical, and asymptotic results are the solid, dashed, and dotted curves, respectively. Results are obtained for flow theory.

mation theory in promoting diffuse modes of stability is now discussed.

The stability predictions for the flow and deformation theories are presented for a constant value for $\Delta\rho g/G\omega$ of 1.41×10^{-4} obtained for a perturbation wavelength of 400π m. Results for an infinitely deep and a 200 m thick substratum are presented in Figures 7a and 7b, respectively. Perfect bond at the basement is assumed. Three important results emerge from that comparison. The first is due to the presence of diamonds at the termination of the curves drawn for the deformation theory. They marked the onset of localized faulting which is now predicted for a stress which is only twice as large in magnitude as the minimum one required for folding (of the order of 80 MPa). The second main result concerns the position of the isocontours in the $(\sigma_0 - \omega H_a)$ plane. The minimum stress to trigger an instability at a given rate of growth is decreased by 25 to 40% as one changes the plasticity theory from flow to deformation. The critical dimensionless thickness ωH_a associated with this minimum is multiplied by a factor of up to 2 during the same operation. The third result in Figure 7 is the surprisingly good predictions of the asymptotic solution (dotted curves) for values of ωH_a of the order of 0.6.

The deformation theory version appears to provide more realistic results than those obtained with the flow theory version of the same plasticity model since folding and localized faulting are now predicted for similar stress magnitudes. For that reason, it is the deformation theory which is adopted in the rest of this section to explore the sensitivity of the predictions to the work hardening, to the in situ stress distribution, and to the redistribution condition at the top surface.

Influence of Work Hardening, in Situ Stress Gradient, and Redistribution

One of the tenets of our plasticity model is the recognition of a work hardening phase after first yield and prior to the approach of a maximum load at which failure would be observed in an experiment. Work hardening is parameterized by a power law shown in Figure 2 for three values of the exponent m. The value of 1 and of infinity corresponds to the elastic case and to the perfectly plastic case, respectively. A value of 5 was chosen for all previous calculations. That value is now changed to 8, tending more toward the perfect plasticity case, which is likely to be realistic for most sedimentary rocks under low confining pressure. Results, presented in Figure 8, compare with those on deformation theory in Figure 7 if a general shift of the isocontours to the right is applied. The reduction in material stiffness resulting from an increase in m leads to a reduction in compressive stress required to trigger the same instability (same rate of growth and wavelength). That reduction in stress magnitude is of the order of 30% but the dominant wavelength for a given rate of growth does not seem to be affected. Note again the agreement between asymptotic (dotted) and exact solution which is, however, not as excellent as in Figure 7.

The influence of the in situ stress gradient with depth is now discussed from the results presented in Figure 9. The in situ stress gradient can be close to the lithostatic gradient ($k_1 = 1$) in sedimentary basins [*Breckels*

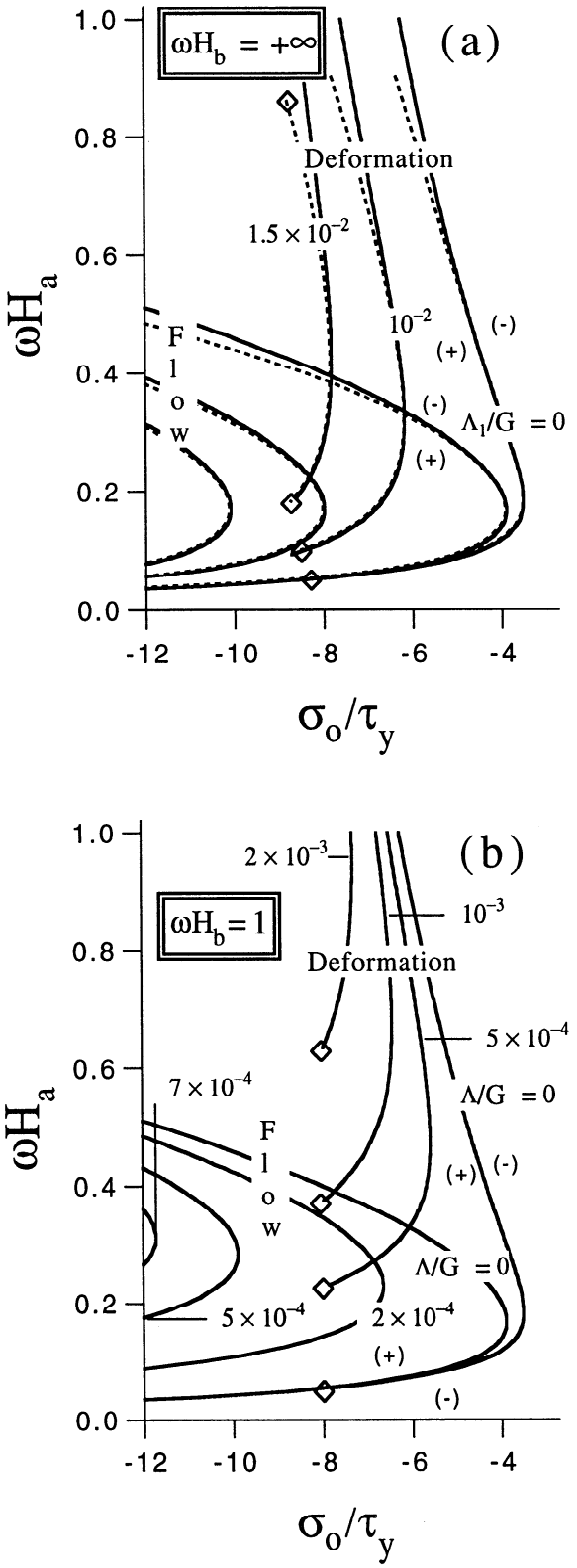

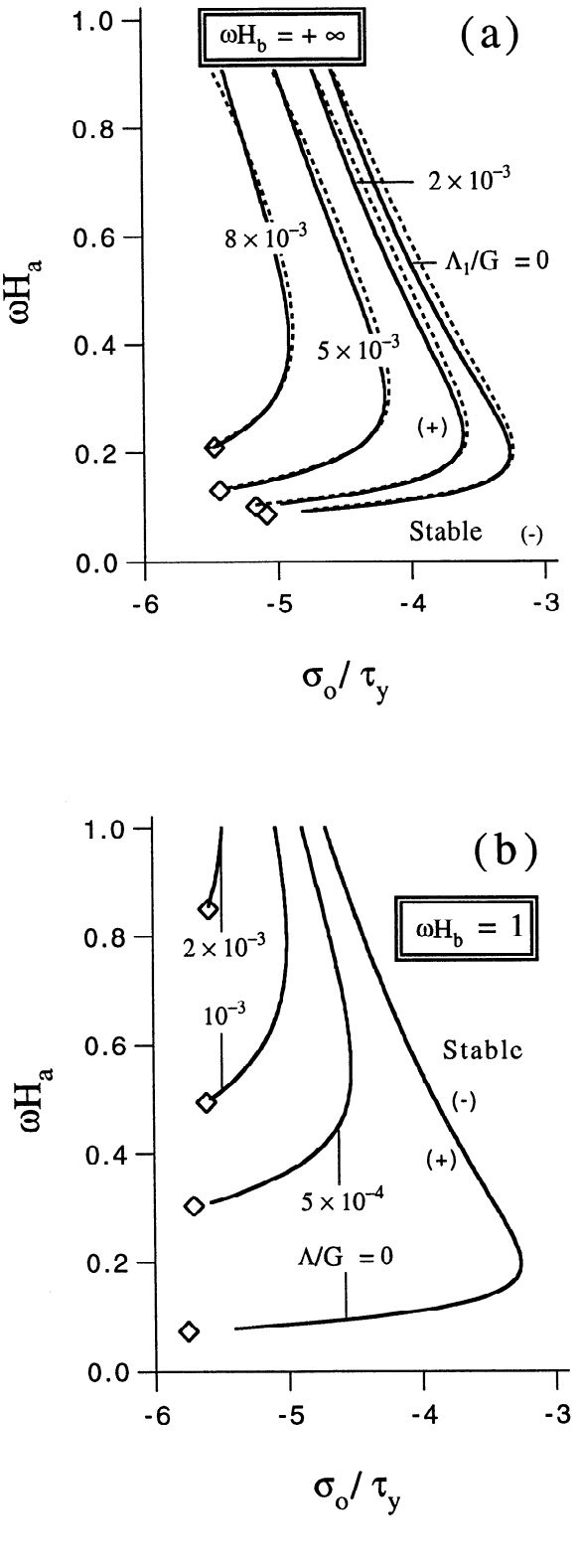

Figure 7. Comparison between the flow and deformation theory versions of *Rudnicki and Rice's* [1975] model for $\Delta\rho g/G\omega = 1.41 \times 10^{-4}$. (a) Results obtained with the finite element method (solid curves) and the asymptotic analysis (dotted curves) for the same three values of the scaled stability exponent Λ_1/G and for an infinitely deep substratum. (b) The stability exponent Λ/G is kept constant and the substratum is 200 m thick. Diamonds indicate the onset of localized faulting.

Figure 8. Influence of the hardening exponent m. (a) The finite element (solid curves) and the asymptotic (dotted curves) iscontours are obtained for a constant scaled stability exponent Λ_1 and an infinitely deep susbstratum. (b) The stability exponent Λ is constant and the substratum thickness is set to 200 m. These results, obtained for $\Delta\rho g/G\omega = 1.41 \times 10^{-4}$ and $m = 8$, should be compared with those obtained with $m = 5$ for deformation theory, which are presented in Figure 7.

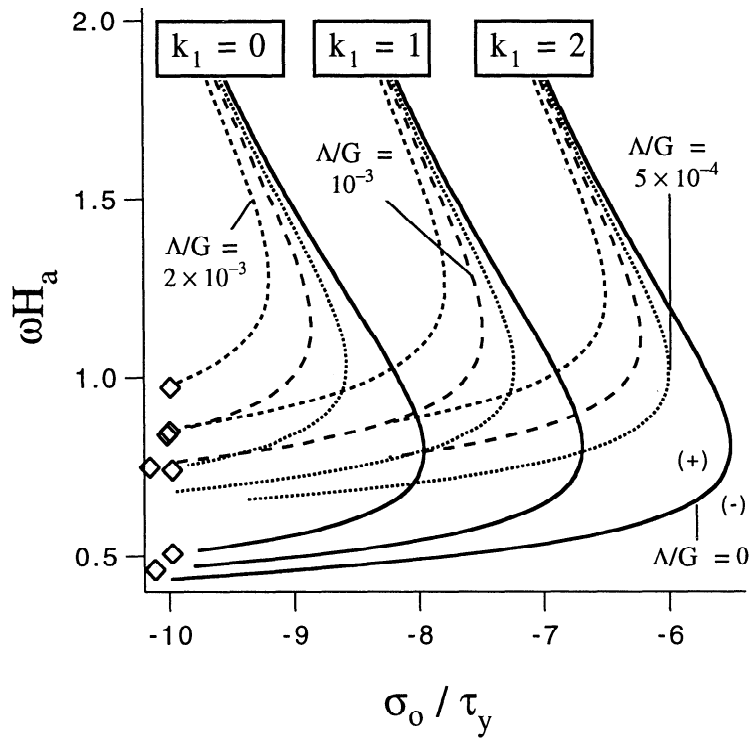

Figure 9. Influence of the stress gradient parameter k_1. Curves of similar type (solid, dotted, or dashed) correspond to the same stability exponent. The finite element results are obtained for deformation theory and for $\Delta\rho g H_a/G = 1.41 \times 10^{-3}$ corrresponding to an overburden thickness of 2 km. The substratum thickness is 1 km, and the boundary condition at the basement is one of slip with no friction. The diamonds, which indicate loss of ellipticity, are not shown for $k_1 = 2$.

and van Eekelen, 1982] but could be twice as large in other areas [*McGarr and Gay,* 1978]. The results are presented for $\Delta\rho g H_a/G$ set to the constant value of 1.41×10^{-3}, obtained for an overburden thickness of 2 km. The cohesion is assumed to be twice as large as before for that thick layer. The substratum thickness is 1 km with a condition of slip with no friction on the basement. To understand the results presented in Figure 9 for the three values of k_1 of 0, 1, and 2, one should recall the in situ stress parameterization depicted in Figure 1. The compressive stress at the interface overburden to substratum is σ_0 in direction 1 since φ is set to zero. The stress magnitude in the same direction is reduced by the amount $k_1 \overset{a}{\rho} g H_a$ at the free surface due to the linear gradient with depth. The value taken by that last expression must be of the order of the compressive stress σ_0 for the in situ stress gradient to have an influence on the stability predictions. It is for that reason that no influence was found for shallow overburden (thickness of order 100 m) and why a thick layer of 2 km was considered here. It is also for that reason that no influence of the stress gradient was detected in paper 1 since instability predictions, based on flow theory, required a large compressive stress (20 times τ_y).

This order of magnitude calculation justifies the geometry and parameter chosen but does not explain the trend observed in Figure 9. There, it seems that the larger the in situ stress gradient the smaller is the magnitude of the compressive stress σ_0 for instability. Indeed, all curves presented in Figure 9 for $k_1 = 1$ and 2 are shifted to the right from the curves obtained for $k_1 = 0$ by an amount of, approximately, 30 and 60 MPa, respectively. That trend is counterintuitive if one estimates the average stress magnitude across the overburden depth from our parameterization. Increasing k_1 reduces that average and should result in an increase and not a decrease in σ_0 if the average compressive stress magnitude was the determinant parameter. It appears that the in situ stress gradient results in an overall bending moment which promotes instability and is more important than the reduction in compressive force. Grounds for that physical argument are found in the asymptotic solution obtained previously for an infinitely deep substratum [*Triantafyllidis and Leroy,* 1994, equation (79)]. There it is seen that the in situ stress gradient acts on the bending stiffness which enters the term of third order in the asymptotic development. That action can only be effective if the stress magnitude is comparable to the tangent moduli. Note that this sensitivity cannot be inferred from the classical beam solution which disregards stress quantities compared to the elastic stiffness.

The last topic of discussion in this section is the role of the redistribution condition at the top surface. That condition, first proposed by *Biot and Odé* [1965], replaces the action of erosion and deposition by assuming that any section of the top surface that is upheaved sustains a positive traction which is equivalent to the

mass displaced and which is supposedly removed by erosion. On any area that subsides, the traction is compressive to replace the weight of new sediments, of same material density as the original overburden material, which should be deposited. The influence of that redistribution condition was discussed by *Triantafyllidis and Leroy* [1994] for the case of an infinitely deep substratum. It was found that shallow overburdens were destabilized even for tectonic stress in the elastic range of deformation. These shallow overburdens, under a zero stress σ_0, must have a dimensionless thickness ωH_a less than $[6(1-\nu)\Delta\rho g/G\omega)]^{1/3}$, from the results for an elastic beam with redistribution at its top [*Leroy and Triantafyllidis,* 1996]. That number is 0.088 for our data set.

Results similar to those discussed above are presented in Figure 10 for the case of a 400π m perturbation wavelength and for an infinitely thick (Figure 10a) or for a 200 m thick (Figure 10b) substratum. Slip with no friction is assumed at the basement. The main feature of Figure 10a is that the isocontours do not have the singular behavior for ωH_a close to zero that was observed previously. As ωH_a decreases, the critical stress on a given isocontour does not have a minimum in magnitude but continues to decrease and enters the region of elastic response, marked by an abrupt change in slope of the isocontour. In Figure 10b, for the 200 m thick substratum, this description has to be amended to recognize that for a large enough rate of growth the shape of the isocontours is the one discussed so far for all previous figures. That change in behavior occurs for a dimensionless rate of growth between 4 and 5 $\times 10^{-5}$ (Figure 10c). For the simplified elastic beam solution with redistribution, this transition is an isocontour intersecting the origin of the coordinate system for a rate of growth Λ/G equal to $\Delta\rho g/G\omega$. That number is 1.41×10^{-4} and is thus 3 times larger then the one estimated by the exact solution. Continuing our analysis of the redistribution condition influence, we note from Figure 10b that any overburden thinner than 400 m is unstable if the tectonic stress distribution generates only elastic deformation. Furthermore, any dimensionless thickness ωH_a below 0.087 is unstable for zero compressive stress. That critical value is very close to the 0.088 found with the plate analysis and provides a non trivial check to our finite element analysis.

Coming back to Figure 10a for a final comment, we note that the asymptotic solution is also used in the extension regime to reveal the initiation of a necking-type instability for a force very close to the one required for the initiation of localized faulting. This remark illustrates the potential usefulness of the asymptotic and of the exact solution in the extension regime which is not explored further in this paper.

Application

The stability predictions are now applied to a prototype for a folded sequence in a sedimentary basin. The prototype has the geometry shown in Figure 1a. The objective of this section is to explain the two stages of folding which have been reported in the field. In the process, it will be shown that a deformation theory of plasticity is required to explain the first folding event in the Albian.

Field Case Description and Motivation

The field structure of interest was revealed by a seismic dip line and is situated 200 km offshore southeast from Cap São Tomé, southeastern Brazilian coast [*Cobbold and Szatmari,* 1991, Figure 3, line E]. That 45 km long line, oriented radially in the Campos salient and presented by *Demercian et al.,* [1993, Figure 5] is sketched in our Figure 11. It has been suggested that gravitational gliding of sediments in the uppermost part of the passive margin results in a downslope contraction which is acting continuously in time. Folding occurred in two stages. The lowermost layers of Cretaceous, 250 m thick, buckled first during the Albian period with a wavelength of 2.5 km. From the end of Cretaceous and through the Tertiary, an anticline developed as the result of buckling on a wavelength of 30 km of the entire sequence which was then 2.5 km thick. The fold development was possible because of a passive inflow of salt. Despite the difficulty of seismic interpretation below the thick salt layer, the base of the salt layer can be assumed to be flat [*Demercian et al.,* 1993].

Two reasons motivate our selection of this field case. First, it is believed that the geometry of the field structure prior to buckling is rather similar to the one adopted for our stability analysis. The prototype proposed for the field case is thus composed of layers of infinite lateral extent with an overburden thickness of 250 m in the Albian or of 2500 m at the end of Cretaceous and during the Tertiary. The use of this prototype for the Campos salient is justified as follows. It is assumed that the instability occurred within the plane of observation, corresponding to the plane strain mode of deformation considered herein. This hypothesis is justified by the radial orientation of the seismic line and the small length of the section compared to the radius of the salient. The thickness of the salt is thought to be of the order of 600 m if the salt inflow in the present dome has been possible by in-plane salt movement only. The salt to basement interface is flat and the absence of deformation in the basement seems to justify its description as a rigid medium. The second reason for our interest in this section of the Campos salient is that folding occurred without any localized faulting. This absence, which we shall try to explain, renders the use of our linear stability analysis valid since the governing equations must be in the elliptic regime. The elastoplasticity model for the overburden material is thus necessary, first to assess the possibility for, or to rule out, localized faulting and second to quantify the importance of the two driving forces for folding, density contrast, and tectonic forces. Note that the lateral contraction is modeled by a lateral compressive stress σ_0 which is an outcome of our stability analysis and can be compared with an estimate of the forces acting in the field that will be provided.

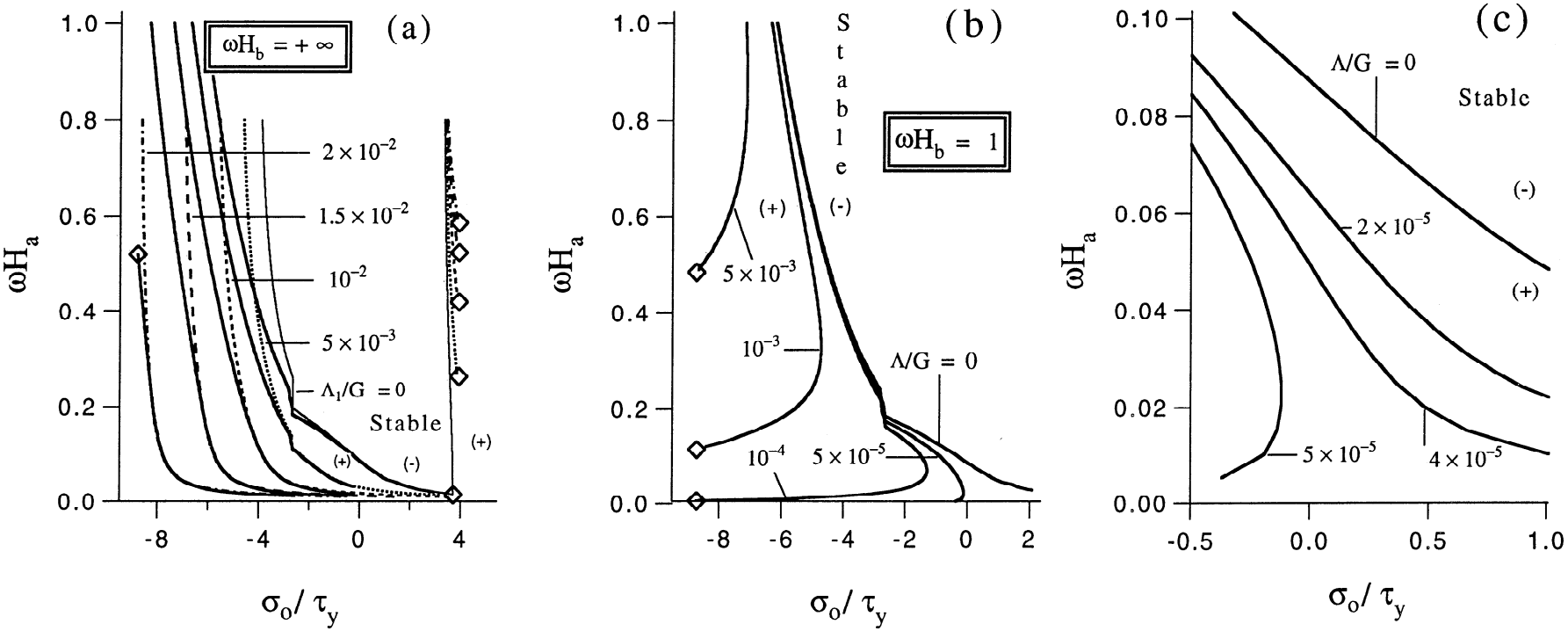

Figure 10. Influence of the redistribution condition at the top surface for a value of $\Delta\rho g/G\omega = 1.41 \times 10^{-4}$. (a) The substratum is infinitely deep and the scaled stability exponent Λ_1 is kept constant. (b) The substratum thickness is set to 200 m and the stability exponent Λ is constant. (c) An enlargment of Figure 10b is shown to pinpoint the change in geometry of the isocontour between 4 and 5 $\times 10^{-5}$. The solid curves are obtained with the finite element solution. Dotted and dashed curves correspond to the asympotic solution, and diamonds mark the onset of localized faulting. Results are obtained for deformation theory.

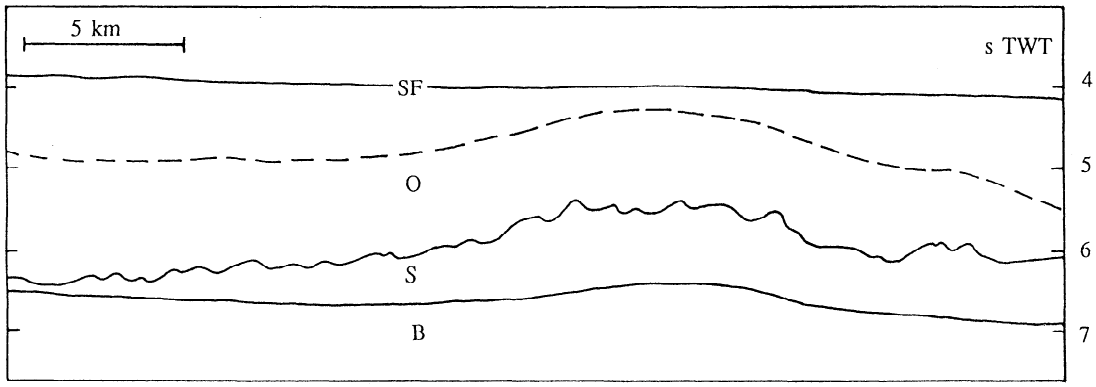

Figure 11. A sketch of the migrated seismic section presented in Figure 5 of [*Demercian et al.*, [1993]. The vertical dimension is in seconds (two-way travel time). The solid lines correspond to the sea floor (SF) and the boundaries between the overburden (O), the substratum (S), and the basement (B). The dashed line shows the limit between the Tertiary and the Cretaceous stratigraphic units.

The in situ stress parameterization presented in Figure 1a and adopted for our prototype is assumed to have prevailed in the field. We first concentrate on the substratum and try to justify this hypothesis. The salt movement during the contraction in the Campos salient is assumed to have been slow enough to produce a hydrostatic stress of state in the salt layer. The validity of that hypothesis is checked by comparing the hydrostatic pressure, which is at least of the order of 5 MPa in the Albian, to the equivalent shear stress, which we now estimate for a Newtonian model. Consider a salt viscosity of 10^{17} Pa/s [*Carter and Hansen*, 1983] and a strain rate of order 10^{-13} due to the simple shear of the 600 m thick salt layer by a displacement of its top of 1 km/Myr. The shear stress is then found to be of the order of a few percent of the pressure and can be disregarded in the analysis. We now consider the overburden and try to motivate the adoption of our stress parameterization. Plane strain deformation is assumed along the seismic line described. If the elastic deformation is disregarded, compared to the permanent strain, and the assumption of zero dilatancy is recalled, then we can conclude that the out of plane stress must be equal to half the vertical stress plus the lateral radial stress. This result is approximated by assigning to the stress angle φ the value $\pi/8$. The two stress gradient parameters k_1 and k_3 are given the value of 1, typical of sedimentary basins. An order of magnitude for the acting compressive stress σ_0 is now proposed. This information is not an input for our predictions but will be used to justify our findings. Assume that the sediments in the radial direction of the salient were gliding toward the structure of interest as a rigid block 100 km long without resistance from the substratum. The slope followed by that block is inferred from Figure 3 of *Cobbold and Szatmari* [1993] to be on average inclined by 1.5°. The fraction of the block weight that generates the compressive stress is thus of the order of 60 MPa.

As a final step in this preliminary part, it is found necessary to provide an explanation for the absence from our discussion of any timescale related to the development of a fold. Such information could permit us to further constrain the conditions that prevailed during folding in the Campos salient. However, they are not available from our analysis for two reasons. First, neither the rate of loading, that governs the contraction, nor the non-Newtonian properties of the salt are accounted for. These two factors are important to quantify the fold development [*Sherwin and Chapple*, 1968; *Fletcher*, 1974] but not for our fold initiation predictions. Second, the linear stability analysis is based on perturbation of infinitesimal size. The observable evolution of the instability, and in particular the fold finite amplitude, can only be estimated from the results of nonlinear analysis. This research direction is under investigation [*Massin*, 1995; *Massin et al.*, 1996] and the set of complete results will be reported later.

Material Properties

This subsection is devoted to the selection of material parameters. A word of caution is necessary since obtaining precise values for the material properties of the sedimentary rocks in the Campos salient is beyond the scope of this paper. The estimates provided are intended to illustrate the potential of our method in explaining the folding events and the absence of localized faulting. With these estimates of the material properties, it is already possible to show how the magnitudes of the stress necessary for instability depend on the model chosen (flow or deformation theory, redistribution or not). These magnitudes are sufficiently different for our conclusions to be insensitive to the exact values of the material parameters.

A short description of the sedimentary record in the Campos basin is provided by *Demercian et al.* [1993]. The sedimentary rocks properties adopted are those found in the previous section with two exceptions. First, the two material densities are now set to 2100 and 2200 kg/m^3. Second, the elastic properties of the sedimentary rock during the Albian are an elastic modulus of 5 GPa whereas a value 10 seems to be more appropriate for the whole sequence during the second stage of the folding.

The Two Folding Events

The stability analysis to be presented is partitioned in two parts. First, it is desirable to understand the initiation of the instability during the Albian. For that purpose, our predictions are proposed for a constant value of $\Delta\rho g H_a/G$ set to 1.2×10^{-4} since the overburden is known to be 250 m thick. The stress σ_0 necessary for the dominant wavelength to be 2.5 km is then calculated. Second, why the buckling development ceased is explained. For that purpose, the observer keeps the wavelength selected previously constant and varies the overburden thickness as it occurred during sedimentation ($\Delta\rho g/\omega G$ is constant). With a similar analysis, it is shown that the second phase of the buckling process could not be initiated without some redistribution at the top surface. All results to be reported in this section are based on the finite element method.

The analysis starts with the prototype for the field structure and the 250 m thick overburden which initiated folding on a wavelength of 2.5 km in the Albian. The stability predictions are presented in Figure 12 for the deformation theory version of *Rudnicki and Rice's* [1975] model and accounting for (dotted curves) or disregarding (solid curves) redistribution. The action of a redistribution superposed to the continuous sedimentation is possible from the observation in Figure 5a of *Demercian et al.* [1993]: the layering on the crest of the small folds appears to be thinner than at the trough. If the dominant perturbation had a wavelength of 2.5 km ($\omega H_a = 0.63$), then the tectonic stress σ_0 must have been close to $-4.3\tau_y$, according to the results in Figure 12. Indeed, it is seen that the isocontour for Λ/G equal to 1.9×10^{-3} has an infinite slope at the point of coordinate (-4.3,0.63) corresponding to the dominant wavelength. The redistribution condition could affect the rate at which the perturbation is initially growing (5×10^{-3}, dotted curve) but seems to be of less importance for the critical stress. That conclusion would be completely different if the perturbation wavelength was twice as large since then erosion would change the stability verdict. Note that the critical stress proposed is not sufficient to initiate localized faulting which is marked by diamonds in Figure 12. To summarize the first part of the analysis, the elastoplasticity model predicts that the instability was initiated for a compressive stress of 43 MPa while localized faulting required as much as 50 MPa of compressive stress. The estimated value for σ_0 in the field of 60 MPa is close to these two values. Note that these results were obtained with the deformation theory. Indeed, predictions with the flow theory indicate that a compressive stress of 140 MPa is necessary for the dimensionless wavenumber 0.63 to be dominant.

The question now debated is the reasons for the arrest of the folding initiated during the Albian and for the generation during the late Cretaceous of the fold with a long wavelength of the order of 30 km. A first explanation for the arrest of the fold development can be found in the nonlinear stability analysis of *Massin*

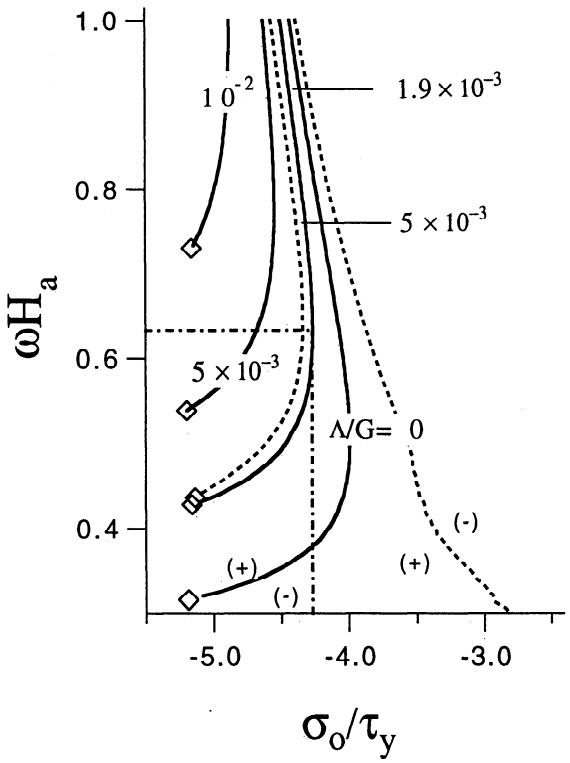

Figure 12. Instability predictions for a prototype of the Campos salient in the Albian with an overburden thickness of 250 m. Results obtained accounting (dotted curves) and disregarding (solid curves) redistribution at the top surface and with the deformation theory version of *Rudnicki and Rice's* [1975] model. For the wavelength of 2.5 km to be dominant, the compression stress σ_0 had to be close to -45 MPa. That value is not sufficient to trigger localized faulting identified by diamonds.

et al. [1996], who showed that an initially unstable equilibrium state will evolve toward a new equilibrium state in the form of a fold of finite amplitude. The amplitude is a function of the compressive stress σ_0. We use another approach here and assume that the dominant wavelength selected was the only possible mode to develop and that the compressive action of the gliding sediments was unaltered with time. Furthermore, we assume that the linear stability argument is still acceptable despite the finite amplitude of the fold. Figure 13 plots the conditions for neutral stability for a wavelength of 2.5 km in the absence (solid line) and in presence of redistribution (dotted curve). If the tectonic compressive stress is kept to the suggested value, then the system is unstable as long as the dimensionless thickness ωH_a is less than 0.73 or 0.80 depending on the action of redistribution. These results suggests that the system became stable once the thickness reached the critical values of 290 or 320 m, the latter value accounting for redistribution.

The onset of the fold with a 30 km long wavelength is now discussed. Results are presented in Figure 13 by a dashed curve obtained with the redistribution condition. The equivalent curve in the absence of erosion

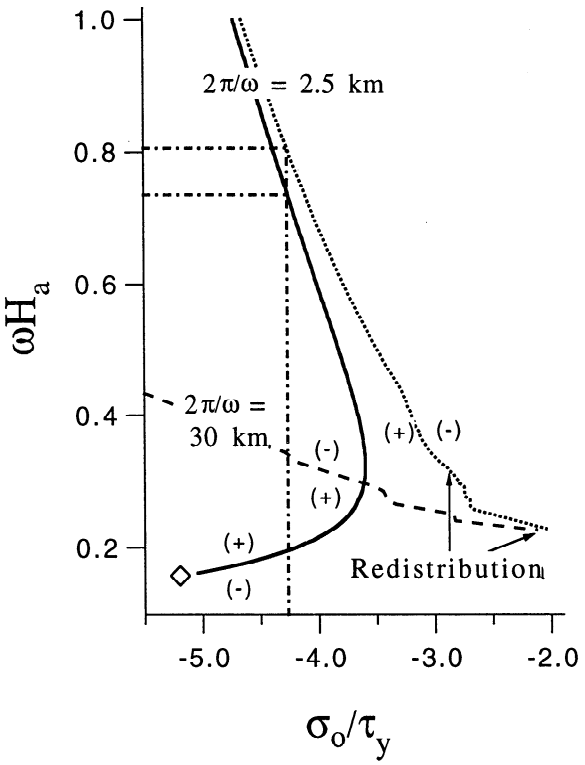

Figure 13. For a constant perturbation wavelength of 2.5 km and 30 km, the range of dimensionless overburden height in the Campos salient for instability is presented as a function of the compressive stress. The curves correspond to neutral stability in the absence (solid) and the presence of redistribution (dotted and dashed) at the top surface. In the absence of redistribution and for the long wavelength perturbation, neutral stability requires localized faulting (not presented here). Redistribution was thus necessary to trigger such a long wavelength mode of instability.

is not presented in Figure 13 since the critical stress required for neutral stability is 40 times larger than τ_y. That finding suggests that it was not possible to initiate folding on such a long wavelength without the action of redistribution. The dashed curve of Figure 13, obtained in the presence of redistribution, reveals that any overburden with a thickness less than 3 km is destabilized for a compressive stress which is amended from the previously suggested value to account for the new lithostatic pressure (σ_0 = -80 MPa). The action of redistribution during the long-wavelength fold development is confirmed by the observation made by *Cobbold and Szatmari* [1991] that the syncline had been filled by sediments during the Tertiary, as it is illustrated in Figure 11.

Conclusion

Two solutions for the stability of the stratified system composed of an elastoplastic overburden, a viscous substratum, and a rigid basement are proposed. The first is analytical and obtained in the absence of gravity effects, and the second, based on the finite element method, approximates with the desired accuracy the exact solution which cannot be obtained analytically. The stratified system studied could be seen as a prototype for studying the initiation of modes of instability such as folding and localized faulting in the context of salt tectonics or at the lithospheric scale. Note that such stability analysis could also be applied to analogue models as it is done by *Leroy and Triantafyllidis* [1997], who discussed the difficulty in reproducing the onset of both localized faulting and of folding with granular materials.

Results are presented in the form of stability exponent isocontours Λ in a plane spanned by the compressive stress σ_0 and the dimensionless wavenumber or overburden thickness ωH_a. The general structure of the solution is reminiscent of the classical solution for an elastic plate on an infinitely deep substratum [*Smoluchowski,* 1909] with the difference that the in situ stress gradient, the nonlinear overburden stiffness, and a possible redistribution condition at the top surface are also accounted for. The asymptotic solution, derived in paper 1, is found to be accurate in all cases considered for values of the small parameter ωH_a as large as 0.4. The analytical solution, obtained disregarding gravity, is also accurate for large value of the dimensionless wavenumber ωH_a. This accuracy is improved for large values of the dimensionless stability exponent Λ/G compared to the dimensionless number $\Delta\rho g/G\omega$, in which $\Delta\rho$ is the density contrast and G the modulus of elasticity in shear.

The validation of the asymptotic solution permits us to confirm some of the results presented in paper 1. The substratum thickness influences by as much as a factor of two the critical stress for instability and by up to 30% the wavelength of the dominant mode. If the substratum thickness is less than 4 times the perturbation wavelength ($\omega H_b \leq 4$), then the type of boundary condition at the basement influences the stability predictions. The dominant wavelength is not affected, but the magnitude of in situ stress necessary to trigger an instability at a positive rate can be increased by up to a factor of 2 if the condition of slip with no friction is replaced by a perfect bond. Another conclusion of that comparison is that folding modes of instability are always found for the smallest magnitude of the compressive stress for all practical cases considered herein. However, surface modes of instability [*Triantafyllis and Lehner,* 1993] cannot be ruled out for very thick overburden.

The comparison between predictions for flow and deformation theories shows the sensitivity of the stability conditions to the details of the constitutive model adopted for the overburden. The presence of small, pervasive faults in the overburden which accommodate part of the deformation by slip, modeled here by the deformation theory, leads to a reduction in the magnitude of the compressive stress required for folding instability. The same trend is observed for the initiation of localized faulting, as already known since the work of *Rudnicki and Rice* [1975]. With that deformation the-

ory, it is found that the in situ stress gradient has a destabilizing effect: increasing the stress gradient leads to a reduction of the average lateral compressive stress magnitude necessary for instability. This influence is explained from the asymptotic solution which reveals that the stabilizing role of the bending stiffness is reduced by the presence of a stress gradient. This result could not be inferred from previously published asymptotic solutions which systematically disregard stress compared to tangent moduli. It is also shown with that deformation theory of plasticity that the redistribution condition at the top surface drastically changes the structure of the stability conditions. In that instance, it is possible to destabilize shallow overburden even with small compressive stress.

The stability predictions are subsequently applied to a folded structure revealed by a seismic survey in the Campos salient, 200 km southest from the Cap Saõ Tomé on the Brazilian coast [*Cobbold and Szatmari*, 1991]. That structure is selected because our model could be considered as a prototype to study the onset of folding, which occurred in the absence of localized faulting and is due to the compressive lateral stress and to the density contrast. It is shown that the compressive stress predicted to initiate buckling in the Albian is close to the one estimated from the field description, if a deformation theory of plasticity is adopted. Furthermore, as sedimentation continues, the stiffness of the overburden increases and the instability is shown to cease if one accepts our stability predictions which disregard the presence of finite amplitude perturbation. The long-wavelength fold triggered during the late Cretaceous is found to result from the combined action of the tectonic compressive force, the density contrast, and an uneven sedimentation which is modeled as a redistribution condition at the top surface [*Biot and Odé*, 1965]. That uneven sedimentation is confirmed by the observation that the syncline was filled by Tertiary sediments [*Demercian et al.*, 1993].

The sensitivity of the stability predictions to the details of the elastoplastic model shows the need to develop, in the future, plasticity models which are appropriate for studies at the tectonic scale. These models should be constructed from a mechanical description of the dominant microscale deformation mechanism that leads to bulk deformation. For example, the micromechanism could be the opening or the sliding along a population of diffuse fractures, initially randomly distributed as discussed by *Lehner and Kachanov* [1995]. Such constitutive relations will improve our modeling capabilities, compared to classical phenomenological laws inherited from the geotechnical literature, and will also provide the means to relate the anisotropic development of pervasive fractures to bulk deformation. The importance of that link for predicting fractured reservoir permeability is discussed by *Leroy and Sassi* [1997].

Appendix: Two Solutions to the Stability Problem

This appendix contains the derivation of two solutions to the stability problem: the first is analytical, obtained in the absence of gravity effects and the second is numerical, based on the finite element method.

Analytical Solution Disregarding Gravity

The motivation to disregard gravity comes from the observation that the zero-order term on the right-hand side of the plate solution (7), $\Delta\rho g/\omega G$, which has typical values of order 10^{-4} to 10^{-5}, becomes negligible compared to sufficiently large rate of growth of the perturbation Λ/G. It is then the tectonic stress and not the density contrast which controls the initiation of the instability. The absence of gravity renders the stress distribution presented in Figure 1 uniform and thus permits the derivation of an analytical solution. The starting point of the derivation of this solution is the Euler-Lagrange equations of the variational statement (3)

$$L_{1111}U_1 - \frac{L_{1122}+L_{1212}}{\omega H_a}\frac{dU_2}{d\xi} - \frac{L_{1221}}{(\omega H_a)^2}\frac{d^2U_1}{d\xi^2} = 0\,,$$
$$L_{2112}U_2 + \frac{L_{2121}+L_{2211}}{\omega H_a}\frac{dU_1}{d\xi} - \frac{L_{2222}}{(\omega H_a)^2}\frac{d^2U_2}{d\xi^2} = 0\,, \quad \text{(A1)}$$

in which the incremental moduli L_{ijkl} are now independent of position in the overburden. The superscript a on the moduli in (A1) and in what follows has been dropped for clarity since no confusion is possible between overburden and substratum. The boundary conditions at the top surface ($\xi = 1$) are

$$L_{1212}U_2 + \frac{1}{\omega H_a}L_{1221}\frac{dU_1}{d\xi} = 0\,,$$
$$-L_{2211}U_1 + \frac{1}{\omega H_a}L_{2222}\frac{dU_2}{d\xi} = 0\,, \quad \text{(A2)}$$

and at the interface between overburden and substratum ($\xi = 0$) are

$$L_{1212}U_2 + \frac{L_{1221}}{\omega H_a}\frac{dU_1}{d\xi} = \Lambda(f_{11}U_1 + f_{12}U_2)\,,$$
$$-L_{2211}U_1 + \frac{L_{2222}}{\omega H_a}\frac{dU_2}{d\xi} = \Lambda(f_{21}U_1 + f_{22}U_2)\,. \quad \text{(A3)}$$

The system of two second-order ordinary differential equations with constant coefficients in (A1) plus the boundary conditions (A2) and (A3) is similar to the one obtained by *Triantafyllidis and Leroy* [1994] for an infinitely deep substratum. The difference between the two systems is the presence in the right-hand side of (A3) of the interface boundary functions. The general solution of (A1) is

$$U_i(\xi) = \sum_{\alpha=1}^{4} V_i^{\alpha}\exp(\omega H_a Z_\alpha \xi)\,, \quad \forall\,\xi \in [0,1]\,, \quad \text{(A4)}$$

in which the four vectors V_i^{α} are the eigenvectors associated with the zero eigenvalue of the system

$$C_{ij}(Z_\alpha)V_i^{\alpha} = 0\,, \quad \text{(A5)}$$

with $C_{ij}(Z_\alpha)$ given by

$$\begin{bmatrix} -L_{1111}+Z_\alpha^2 L_{1221} & Z_\alpha(L_{1122}+L_{1212}) \\ -Z_\alpha(L_{2211}+L_{2121}) & -L_{2112}+Z_\alpha^2 L_{2222} \end{bmatrix} . \quad \text{(A6)}$$

The scalars Z_α are the four roots of the polynomial $\det[C_{ij}(Z)] = 0$. The system C_{ij} is obtained by inserting the general solution (A4) in the two differential equations (A1). The amplitudes of the eigenvectors V_i^α are constrained to satisfy the four boundary conditions (A2) and (A3) leading to

$$\sum_{\alpha=1}^{4} M_{\beta\alpha} V_1^\alpha = 0 , \quad \text{(A7)}$$

in which the components of $M_{\beta\alpha}$ are

$$\begin{aligned} M_{1\alpha} &= [L_{1212}\beta_\alpha + L_{1221}Z_\alpha]\exp(\omega H_a Z_\alpha) , \\ M_{2\alpha} &= [-L_{2211} + \beta_\alpha L_{2222} Z_\alpha]\exp(\omega H_a Z_\alpha) , \\ M_{3\alpha} &= L_{1221}Z_\alpha + \beta_\alpha L_{1212} - \Lambda(f_{11}+\beta_\alpha f_{12}) , \\ M_{4\alpha} &= L_{2222}Z_\alpha\beta_\alpha - L_{2211} - \Lambda(f_{21}+\beta_\alpha f_{22}) . \end{aligned} \quad \text{(A8)}$$

The four scalars β_α introduced in (A8) take the values $-C_{11}(Z_\alpha)/C_{12}(Z_\alpha)$.

The consecutive resolution of (A7) ($\det[M_{\beta\alpha}(\Lambda)] = 0$) and (A1) permits to construct the four eigenvectors and to determine the stability exponent Λ, which are at the basis of the general solution to the stability problem in the absence of gravity.

The Finite Element Solution

The finite element solution provides the means to assess the accuracy of the asymptotic solution, to determine the range of validity of the analytical solution in absence of gravity, and to check if modes of instability other than bending modes could be relevant. Such modes include interfacial instabilities [*Triantafyllidis and Lehner,* 1993] which require a fine spatial resolution close to the interface with the substratum.

The overburden thickness is partitioned in N finite elements, with the last node being at the interface with the substratum to simplify the presentation of the argument that follows. These elements are chosen to be three noded with the same interpolation for the eigenvector $\mathbf{U}$ and the variations $\delta\mathbf{U}$

$$\mathbf{U} \simeq \sum_{l=1}^{N} N_l \tilde{\mathbf{U}}_l \quad , \quad \delta\mathbf{U} \simeq \sum_{l=1}^{N} N_l \delta\tilde{\mathbf{U}}_l , \quad \text{(A9)}$$

in terms of the shape functions based on Legendre polynomials N_l and the nodal quantities $\tilde{\mathbf{U}}_l$ and $\delta\tilde{\mathbf{U}}_l$. The introduction of this interpolation in the variational expression (3) leads to a banded system of $2N$ equations which is written as

$$\begin{bmatrix} \mathbf{K}_{lm} & \mathbf{K}_{lN} \\ \mathbf{K}_{Nm} & \mathbf{K}_{NN} + \Lambda\mathbf{M}_{NN} \end{bmatrix} \begin{bmatrix} \tilde{\mathbf{U}}_m \\ \tilde{\mathbf{U}}_N \end{bmatrix} = \begin{bmatrix} \mathbf{0} \\ \mathbf{0} \end{bmatrix} , \quad \text{(A10)}$$

in which every $\mathbf{K}_{lm}$ and $\mathbf{M}_{NN}$ is a 2×2 array. The subscripts m and l range from 1 to $N-1$. The matrix $\mathbf{M}_{NN}$ has components $f_{ij}/\omega H_a$ in which the functions f_{ij}, defined in (4)-(5), introduce the influence of the substratum thickness and of the boundary conditions at the basement.

The problem presented in (A10) is a generalized algebraic eigenvalue analysis for a non-symmetric system. Its solution computation is facilitated by expressing the $(N-1)$ first unknown eigenvectors $\tilde{\mathbf{U}}_m$ in terms of the last ones positioned on the interface, $\tilde{\mathbf{U}}_N$. This operation is done with the use of the first equation in (A10) and the simplified eigenvector problem then reads

$$\left\{\mathbf{K}_{NN} - \mathbf{K}_{Nl}\mathbf{K}_{lm}{}^{-1}\mathbf{K}_{mN} + \Lambda\mathbf{M}_{NN}\right\}\tilde{\mathbf{U}}_N = \mathbf{0} , \quad \text{(A11)}$$

from which the critical Λ is found as the eigenvalue with the largest real part of the 2×2 system.

Acknowledgments. This work was initiated while one of us (Y.M.L.) was working for Shell Research KSEPL (now RTS), Rijswijk, Holland. Helpful discussions with J.L. Urai (University of Aachen, Germany) and D. Nieuwland (RTS) are gratefully acknowledged. The field case considered was kindly suggested by P. Cobbold (University of Rennes, France). The continuous encouragements and the contribution of F.K. Lehner (University of Bonn, Germany) was essential to the realization of this work. This work was completed during the visit in 1996 of Y.M.L. at the University of Michigan. The hospitality of the Department of Aerospace Engineering is gratefully acknowledged. Permission to publish this paper was granted by Shell Internationale Research Maatschappij BV.

References

Biot, M.A., and H. Odé, Theory of gravity instability with variable overburden and compaction, *Geophysics, 30*, 213-227, 1965.

Breckels, I.M., and H.A.M. van Eekelen, Relationship between horizontal stress and depth in sedimentary basins, *J. Pet. Technol., 9*, 2191-2199, 1982.

Carter, N.L., and F.D. Hansen, Creep of rocksalt, *Tectonophysics, 92*, 275-333, 1983.

Cobbold, P.R., and P. Szatmari, Radial gravitational gliding on passive margins, *Tectonophysics, 188*, 249-289, 1991.

Daudré, B., and S. Cloetingh, Numerical modelling of salt diapirism: Influence of the tectonic regime, *Tectonophysics, 240*, 59-79, 1994.

Demercian, S., P. Szatmari, and P.R. Cobbold, Style and pattern of salt diapirs due to thin-skinned gravitational gliding, Campos and Santos basins, offshore Brazil, *Tectonophysics, 228*, 393-433, 1993.

Drucker, D.C., and W. Prager, Soil mechanics and plastic analysis or limit design, *Q. J. Mech. Appl. Math., 10*, 157-165, 1952.

Fletcher, R.C., Wavelength selection in the folding of a single layer with power-law rheology, *Am. J. Sci., 274*, 1029-1043, 1974.

Hill, R., A general theory of uniqueness and stability in elasic-plastic solids, *J. Mech. Phys. Solids, 6*, 236-249, 1958.

Lehner, F.K. and M.L. Kachanov, On the stress-strain relations for cracked elastic materials in compression, in *Mechanics of Jointed and Faulted Rock*, edited by H.P. Rossmanith, A.A. Balkema, Rotterdam, 49-61, 1995.

Leroy, Y., and M. Ortiz, Finite element analysis of strain localization in frictional materials, *Int. J. Numer. Anal. Methods Geomech., 13*, 53-74, 1989.

Leroy, Y.M., and W. Sassi, A plasticity model for discontinua, in *Aspects of Tectonic Faulting, Lecture Notes in Earth Sciences,* edited by F.K. Lehner, G. Riedmueller and E. Wallbrecher, Springer-Verlag, New York, in press, 1997.

Leroy, Y.M., and N. Triantafyllidis, Stability of a frictional, cohesive layer on a substratum: Variational formulation and asymptotic solution, *J. Geophys. Res., 101,* 17,795-17,811, 1996.

Leroy, Y.M., and N. Triantafyllidis, Onset of folding and faulting in density-stratified systems: an elastoplastic model, in *Aspects of Tectonic Faulting, Lecture Notes in Earth Sciences,* edited by F.K. Lehner, G. Riedmueller and E. Wallbrecher, Springer-Verlag, New York, in press, 1997.

Massin, P., On the stability of strain-rate dependent solids and structures, Ph.D. dissertation, Univ. of Mich., Ann Arbor, 1995.

Massin, P., N. Triantafyllidis, and Y.M. Leroy, Stability of density-stratified two-layer system, *C. R. Acad. Sci., Sér. IIa, 322,* 407-413, 1996.

McAdoo, D.C., and D.T. Sandwell, Folding of the oceanic lithosphere, *J. Geophys. Res., 90,* 8563-8569, 1985.

McGarr, A., and N.C. Gay, State of stress in the earth's crust, *Annu. Rev. Earth Planet. Sci., 6,* 405-436, 1978.

Nettleton, L.L., and A. Elkins, Geologic models made from granular materials, *Eos Trans. AGU, 28,* 451-466, 1947.

Ogden, R.W., *Non-linear elastic deformations,* Ellis Horwood, Chichester, England, 1984.

Poliakov, A.N.B., Y. Podladchikov, and C. Talbot, Initiation of salt diapirs with frictional overburdens: Numerical experiments, *Tectonophysics, 228,* 199-210, 1993.

Ramberg, H.R., and O. Stephansson, Compression of floating elastic and viscous plates affected by gravity, a basis for discussing crustal buckling, *Tectonophysics, 1,* 101-120, 1964.

Rudnicki, J.W., The inception of faulting in a rock mass with a weakened zone, *J. Geophys. Res., 82,* 844-854, 1977.

Rudnicki, J.W., and J.R. Rice, Conditions for the localization of the deformation in pressure-sensitive dilatant materials, *J. Mech. Phys. Solids, 23,* 371-394, 1975.

Shanley, F.R., Inelastic column theory, *J. Aeronaut. Sci., 14,* 261-267, 1947.

Sherwin, J.A., and W.N. Chapple, Wavelengths of single layer folds: A comparison between theory and observation, *Am. J. Sci., 266,* 167-179, 1968.

Smoluchowski, M., Über ein gerrisses Stabilitätsproblem der Elastizitätslehre und dessen Beziehung zur Entsehung von Faltengebirgen, *Abhandl. Akad. Wiss Krakau, Math. Kl.* 3-20, 1909.

Stewart, S.A., and M.P. Coward, Genetic interpretation and mapping of salt structures, *First Break, 14,* 135-141, 1996.

Stören, S., and J.R. Rice, Localized necking in thin sheets, *J. Mech. Phys. Solids, 23,* 421-441, 1975.

Triantafyllidis, N., and F. K. Lehner, Interfacial instability of density-stratified two-layer systems under initial stress, *J. Mech. Phys. Solids, 41,* 117-142, 1993.

Triantafyllidis, N., and Y.M. Leroy, Stability of a frictional material layer resting on a viscous half-space, *J. Mech. Phys. Solids, 42,* 51-110, 1994.

van Keken, P.E., C.J. Spiers, A.P van den Berg, and E.J. Muyzert, The effective viscosity of rocksalt: Implementation of steady-state creep laws in numerical models of salt diapirism, *Tectonophysics, 225,* 457-476, 1993.

Vendeville, B.C., and M.P.A. Jackson, The rise of diapirs during thin-skinned extension, *Mar. Pet. Geol., 9,* 331-353, 1992.

Wallace, M.H., and H.J. Melosh, Buckling of a pervasively faulted lithosphere, *Pure Appl. Geophys., 142,* 239-261, 1994.

Y.M. Leroy, Laboratoire de Mécanique des Solides, CNRS, URA 317, Ecole Polytechnique, Palaiseau 91128 Cedex, France. (email:leroyy@athena.polytechnique.fr)

N. Triantafyllidis, Department of Aerospace Engineering, University of Michigan, Ann Arbor, MI 48109-2140. (email:nick@engin.umich.edu)

(Received August 16, 1996; revised April 16, 1997; accepted May 9, 1997.)